A population-level invasion by transposable elements triggers genome expansion in a fungal pathogen

Ursula Oggenfuss[1], Thomas Badet[1], Thomas Wicker[2], Fanny E. Hartmann[3,4], Nikhil K. Singh[1], Leen N. Abraham[1], Petteri Karisto[4,6], Tiziana Vonlanthen[4], Christopher C. Mundt[5], Bruce A. McDonald[4], Daniel Croll[1,*]

[1] Laboratory of Evolutionary Genetics, Institute of Biology, University of Neuchâtel, 2000 Neuchâtel, Switzerland
[2] Institute for Plant and Microbial Biology, University of Zurich, Zurich, Switzerland
[3] Ecologie Systématique Evolution, Bâtiment 360, Univ. Paris-Sud, AgroParisTech, CNRS, Université Paris-Saclay, 91400 Orsay, France
[4] Plant Pathology, Institute of Integrative Biology, ETH Zurich, Zurich, Switzerland
[5] Department of Botany and Plant Pathology, Oregon State University, Corvallis, OR 97331-2902, USA
[6] Department of Evolutionary Biology and Environmental Studies, University of Zurich, Zurich, Switzerland

[*] Author for correspondence: daniel.croll@unine.ch

Running title: Transposable element invasion triggers genome expansion

ABSTRACT

Genome evolution is driven by the activity of transposable elements (TEs). The spread of TEs can have deleterious effects including the destabilization of genome integrity and expansions. However, the precise triggers of genome expansions remain poorly understood because genome size evolution is typically investigated only among deeply divergent lineages. Here, we use a large population genomics dataset of 284 individuals from populations across the globe of *Zymoseptoria tritici*, a major fungal wheat pathogen. We built a robust map of genome-wide TE insertions and deletions to track a total of 2'456 polymorphic loci within the species. We show that purifying selection substantially depressed TE frequencies in most populations but some rare TEs have recently risen in frequency and likely confer benefits. We found that specific TE families have undergone a substantial genome-wide expansion from the pathogen's center of origin to more recently founded populations. The most dramatic increase in TE insertions occurred between a pair of North American populations collected in the same field at an interval of 25 years. We find that both genome-wide counts of TE insertions and genome size have increased with colonization bottlenecks. Hence, the demographic history likely played a major role in shaping genome evolution within the species. We show that both the activation of specific TEs and relaxed purifying selection underpin this incipient expansion of the genome. Our study establishes a model to recapitulate TE-driven genome evolution over deeper evolutionary timescales.

50 **INTRODUCTION**

51 Transposable elements (TEs) are mobile repetitive DNA sequences with the ability to independently
52 insert into new regions of the genome. TEs are major drivers of genome instability and epigenetic
53 change (Eichler & Sankoff, 2003). Insertion of TEs can disrupt coding sequences, trigger
54 chromosomal rearrangements, or alter expression profiles of adjacent genes (Lim, 1988; Petrov *et al.*,
55 2003; Slotkin & Martienssen, 2007; Hollister & Gaut, 2009; Oliver *et al.*, 2013). Hence, TE activity
56 can have phenotypic consequences and impact host fitness. While TE insertion dynamics are driven
57 by the selfish interest for proliferation, the impact on the host can range from beneficial to highly
58 deleterious. The most dramatic examples of TE insertions underpinned rapid adaptation of populations
59 or species (Feschotte, 2008; Chuong *et al.*, 2017), particularly following environmental change or
60 colonization events. Beneficial TE insertions are expected to experience strong positive selection and
61 rapid fixation in populations. However, most TE insertions have neutral or deleterious effects upon
62 insertions. Purifying selection is expected to rapidly eliminate deleterious insertions from populations
63 unless constrained by genetic drift (Walser *et al.*, 2006; Baucom *et al.*, 2008; Cridland *et al.*, 2013;
64 Stuart *et al.*, 2016; Lai *et al.*, 2017; Stritt *et al.*, 2017). Additionally, genomic defense mechanisms can
65 disable transposition activity. Across eukaryotes, epigenetic silencing is a shared defense mechanism
66 against TEs (Slotkin & Martienssen, 2007). Fungi evolved an additional and highly specific defense
67 system introducing repeat-induced point (RIP) mutations into any nearly identical set of sequences.
68 The relative importance of demography, selection and genomic defenses determining the fate of TEs
69 in populations remain poorly understood.

70

71 A crucial property predicting the invasion success of TEs in a genome is the transposition rate. TEs
72 tend to expand through family-specific bursts of transposition followed by prolonged phases of
73 transposition inactivity. Bursts of insertions of different retrotransposon families were observed across
74 eukaryotic lineages including *Homo sapiens*, *Zea mays*, *Oryza sativa* and *Blumeria graminis* (Shen *et*
75 *al.*, 1991; SanMiguel *et al.*, 1998; Eichler & Sankoff, 2003; Lu *et al.*, 2017; Frantzeskakis *et al.*, 2018).
76 Prolonged bursts without effective counter-selection are thought to underpin genome expansions. In

77 the symbiotic fungus *Cenococcum geophilum*, the burst of TEs resulted in a dramatically expanded
78 genome compared to closely related species (Peter *et al.*, 2016). Similarly, a burst of a TE family in
79 brown hydras led to an approximately three-fold increase of the genome size compared to related
80 hydras (Wong *et al.*, 2019). Across the tree of life, genome sizes vary by orders of magnitude and
81 enlarged genomes invariably show hallmarks of historic TE invasions (Kidwell, 2002). Population
82 size variation is among the few correlates of genome size across major groups, suggesting that the
83 efficacy of selection plays an important role in controlling TE activity (Lynch, 2007). Reduced
84 selection efficacy against deleterious TE insertions is expected to lead to a ratchet-like increase in
85 genome size. In fungi, TE-rich genomes often show an isochore structure alternating gene-rich and
86 TE-rich compartments (Rouxel *et al.*, 2011). TE-rich compartments often harbor rapidly evolving
87 genes such as effector genes in pathogens or resistance genes in plants (Raffaele & Kamoun, 2012;
88 Jiao & Schneeberger, 2019). Taken together, incipient genome expansions are likely driven by
89 population-level TE insertion dynamics.
90
91 The fungal wheat pathogen *Zymoseptoria tritici* is one of the most important pathogens on crops
92 causing high yield losses (Torriani *et al.*, 2015). The genome is completely assembled and shows size
93 variation between individuals sampled across the global distribution range (Feurtey *et al.*, 2020; Badet
94 *et al.*, 2020) (Goodwin *et al.*, 2011). The TE content of the genome shows a striking variation of 17-
95 24% variation among individuals (Badet *et al.*, 2020). *Z. tritici* recently gained major TE-mediated
96 adaptations to colonize host plants and tolerate environmental stress (Omrane *et al.*, 2015, 2017;
97 Krishnan *et al.*, 2018; Meile *et al.*, 2018). Clusters of TEs are often associated with genes encoding
98 important pathogenicity functions (*i.e.* effectors), recent gene gains or losses (Hartmann & Croll,
99 2017), and major chromosomal rearrangements (Croll *et al.*, 2013; Plissonneau *et al.*, 2016).
100 Transposition activity of TEs also had a genome-wide impact on gene expression profiles during
101 infection (Fouché *et al.*, 2019). The well-characterized demographic history of the pathogen and
102 evidence for recent TE-mediated adaptations make *Z. tritici* an ideal model to recapitulate the process
103 of TE insertion dynamics, adaptive evolution and changes in genome size at the population level.
104

105 Here, we retrace the population-level context of TE insertion dynamics and genome size changes
106 across the species range by analyzing populations sampled on four continents for a total of 284
107 genomes. We developed a robust pipeline to detect newly inserted TEs using short read sequencing
108 datasets. Combining analyses of selection and knowledge of the colonization history of the pathogen,
109 we tested whether population bottlenecks were associated with substantial changes in the TE content
110 and the size of genomes.
111
112

113 # RESULTS

114 ## A DYNAMIC TE LANDSCAPE SHAPED BY STRONG PURIFYING SELECTION

115 To establish a comprehensive picture of within-species TE dynamics, we analyzed 284 genomes from
116 a worldwide set of six populations spanning the distribution range of the wheat pathogen *Z. tritici*. To
117 ascertain the presence or absence of TEs across the genome, we developed a robust pipeline (Figure
118 1A). In summary, we called TE insertions by identifying reads mapping both to a TE sequence and a
119 specific location in the reference genome. Then, we assessed the minimum sequencing coverage to
120 reliably recover TE insertions, tested for evidence of TEs using read depth at target site duplications,
121 and scanned the genome for mapped reads indicating gaps at TE loci. We found robust evidence for a
122 total of 18’864 TE insertions grouping into 2’465 individual loci. More than 30% of these loci have
123 singleton TEs (*i.e.* this locus is only present in one isolate; Figure 2B, Supplementary Table S3). An
124 overwhelming proportion of loci (2’345 loci or 95.1%) have a TE frequency below 1%. This pattern
125 strongly supports the hypothesis that TEs actively copy into new locations but also indicates that strong
126 purifying selection maintains nearly all TEs at low frequency (Figure 2B). We found a higher density
127 of TE loci on accessory chromosomes, which are not shared among all isolates of the species,
128 compared to core chromosomes (Figure 2C). This suggests relaxed selection against TE insertion on
129 the functionally dispensable accessory chromosomes.
130

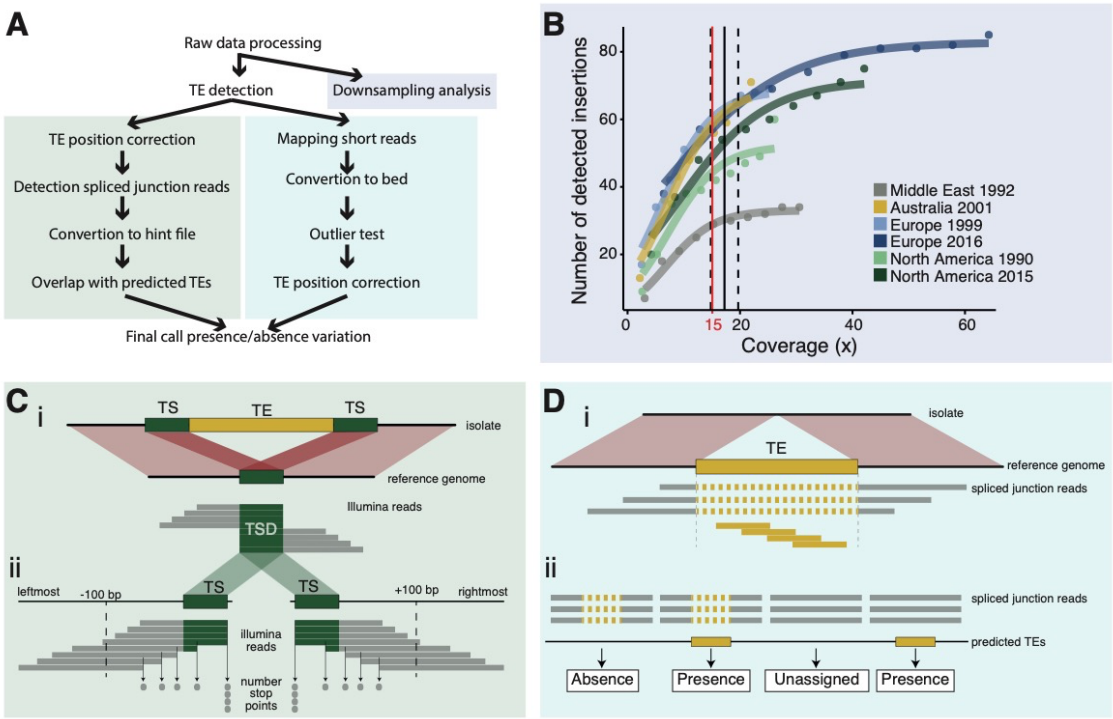

Figure 1: Robust discovery and validation of transposable element (TE) insertions: (A) General analysis pipeline. (B) Read depth down-sampling analysis for one isolate per population with an average coverage of the population. The vertical black line indicates the coverage at which on average 90% of the maximally detectable variants were recovered. Dashed black lines indicate the standard error. The threshold for a minimal mean coverage was set at 15X (red line). (C) Validation of insertions not present in the reference genome. (i) TE insertions that are not present in the reference genome show a duplication of the target site and the part of the reads that covers the TE will not be mapped against the reference genome. We thus expect reads to map to the TE surrounding region and the target site duplication but not the TE itself. At the target site, a local duplication of read depth is expected. (ii) We selected all reads in an interval of 100 bp up- and downstream including the target site duplication to detect deviations in the number of reads terminating near the target site duplication. (D) Validation of insertions present in the reference genome. (i) Analyses read coverage at target site duplications. (ii) Synthesis of evidence from ngs_te_mappr and split read mapping to determine TE presence or absence.

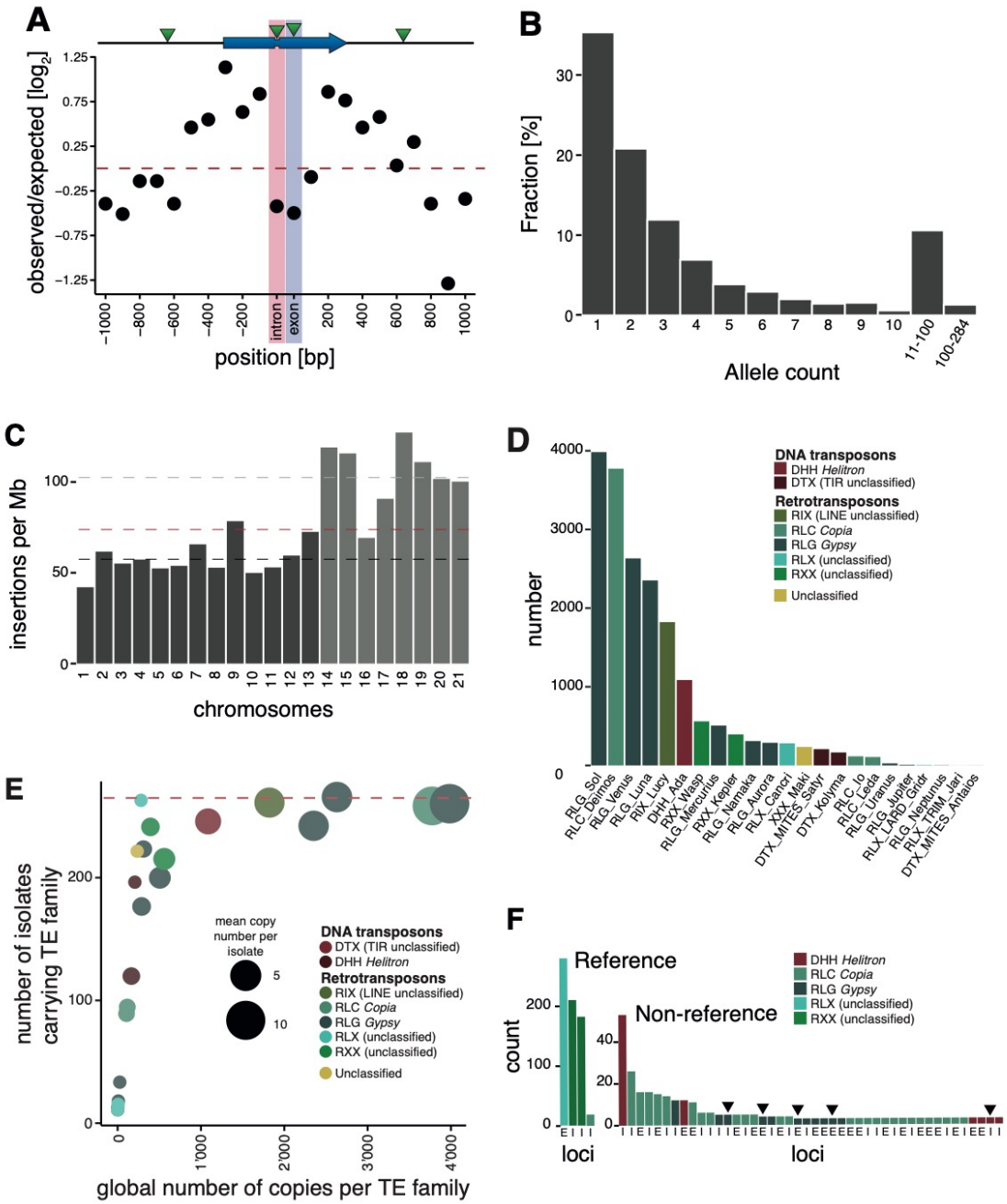

Figure 2: Transposable element (TE) landscape across populations. (A) Number of TE insertions 1 kb up- and downstream of genes on core chromosomes including introns and exons (100 bp windows). (B) Allele frequencies of the TE insertions across all isolates. (C) TE insertions per Mb on core chromosomes (dark) and accessory chromosomes (light). Dashed lines represent mean values. Red: global mean of 75.65 insertions/Mb, dark: core chromosome mean of 58 TEs/Mb, light: accessory chromosome mean of 102.24 insertions/Mb). (D) Number of TE insertions per family. (E) TE frequencies among isolates and copy numbers across the genome. The red line indicates the maximum number of isolates (n = 284). (F) TE insertions into introns and exons that are present in the reference genome and TEs absent from the reference genome but present in more than two copies in the populations. A hexagon indicates that the insertion was found in only one population, all other insertions were found in at least two populations. I = intron insertion, E = exon insertion.

157 TEs grouped into 23 families and 11 superfamilies, with most TEs belonging to class
158 I/retrotransposons (*n* = 2175; Supplementary Figure S4A; Figure 2D). *Gypsy* (*n* = 1'483) and *Copia*
159 (*n* = 623) elements constitute the largest long terminal repeats (LTR) superfamilies. Class II/DNA
160 transposons are dominated by *Helitron* (*n* = 249). TE families shared among less isolates tend to show
161 also lower copy numbers as expected (Figure 2E).
162
163 We detected 153 TE insertions into genes with most insertions being singletons (*n* = 68) or at very
164 low frequency (Figure 2F). Overall, TE insertions into exonic sequences were less frequent than
165 expected compared to insertions into up- and downstream regions, which is consistent with effective
166 purifying selection (Figure 2A). Insertions into introns were also strongly under-represented, likely
167 due to the small size of most fungal introns (~ 50-100 bp) and the high probability of disrupting
168 splicing or adjacent coding sequences. We also found that insertions 800-1000 bp away from coding
169 sequences of a focal gene were under-represented. Given the high gene density, with an average
170 spacing between genes of 1,744 kb, TE insertions within 800-1000 bp of a coding gene tend to be near
171 adjacent genes already. Taken together, TEs in the species show a high degree of transposition activity
172 and are subject to strong purifying selection.
173
174 DETECTION OF CANDIDATE TE LOCI UNDERLYING RECENT ADAPTATION
175 The TE transposition activity can generate adaptive genetic variation. To identify the most likely
176 candidate loci, we analyzed insertion frequency variation among populations as an indicator for recent
177 selection. Across all populations, the insertion frequencies differed only weakly with a strong skew
178 towards extremely low F_{ST} values (mean = 0.0163; Figure 3A, 3C). High F_{ST} loci tend to have high
179 TE frequencies in either the North American population from 2015 or the Australian population. Given
180 our population sampling, we tested for the emergence of adaptive TE insertions either in the North
181 American or European population pairs. Hence, we selected loci having low TE insertion frequencies
182 (< 5%) in all populations except either the recent North American or European population (> 20%)
183 (Figure 3B). Based on these criteria, we obtained 26 candidate loci possibly underlying local
184 adaptation in the North American populations with 22 loci showing retrotransposon insertions, three

185 *Helitron*, and one DNA TIR transposon. In parallel, we found six loci of retrotransposons possibly
186 underlying local adaptation in the European populations (Figure 4A and Supplementary Table S4). To
187 further analyze evidence for TE-mediated adaptive evolution, we screened the whole-genome
188 sequencing datasets for evidence of selective sweeps using selection scans. Out of all 32 loci showing
189 signatures of local adaptation in North American or European populations, we found five loci
190 overlapping selective sweep regions. All TEs inserted in regions of selective sweeps are
191 retrotransposons including *Copia* and *Gypsy* elements.

192

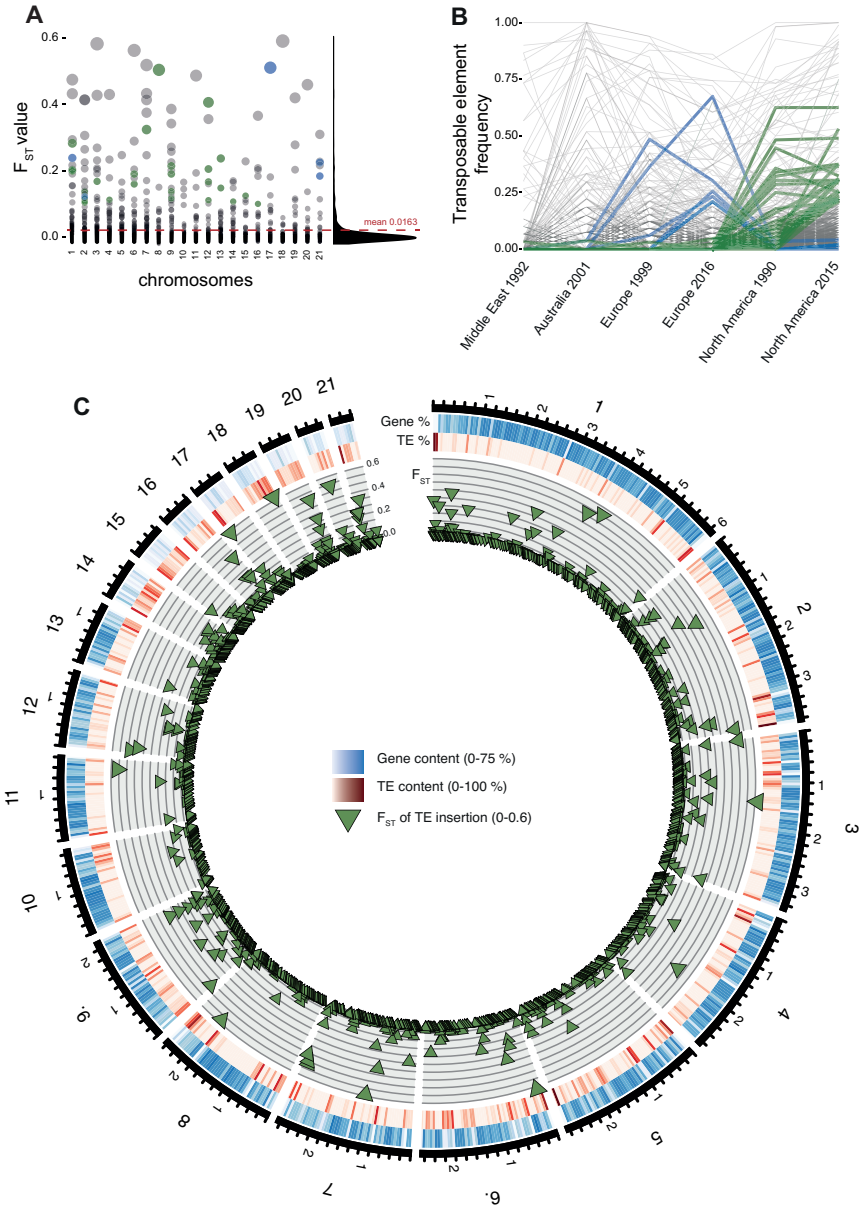

193

194 **Figure 3: Differentiation in transposable element insertions frequencies across the genome**. (A) Global
195 pairwise F_{ST} distributions shown across the 21 chromosomes. The red horizontal line indicates the mean F_{ST} (=

196 0.0163). TEs with a strong local short-term frequency difference among populations are highlighted (blue:
197 increase in Europe; green: increase in North America). (B) Allele frequency changes between the populations.
198 The same TE loci as in panel A are highlighted. (C) Circos plot describing from the outside to the inside: The
199 black line indicates chromosomal position in Mb. Blue bars indicate the gene density in windows of 100 kb with
200 darker blue representing higher gene density. Red bars indicate the TE density in windows of 100 kb with a
201 darker red representing higher TE density. Green triangles indicate positions of TE insertions with among
202 population F_{ST} value shown on the y-axis.
203

204 We focused on five TE insertion loci in proximity to genes with a function likely associated with
205 fungicide resistance or host adaptation. A TE insertion is 105 bp downstream of a major facilitator
206 superfamily (MFS) transporter gene and 644 bp upstream of a TATA box (Figure 4B). MFS
207 transporters can contribute to the detoxification of antifungal compounds in the species (Omrane *et*
208 *al.*, 2017). The inserted *Helitron* TE was only found in North American populations (Figure 4G). The
209 TE insertion occurred in a gene-rich, TE-poor region and the $F_{ST} = 0.51$ was one of the highest values
210 of all TE loci (Figure 4C). Generally, the *Helitron* increased strongly in copy number from the Israel
211 to the North American populations (Figure 4D, 4F). The phylogeny of the gene encoding the MFS
212 showed a high degree of similarity for all isolates carrying the *Helitron* insertion compared to the
213 isolates lacking the *Helitron* (Figure 4E). This is consistent with a rapid rise in frequency of the
214 haplotype carrying the *Helitron* driven by positive selection. A second TE insertion that was only
215 found in the two North American populations also contains a *Helitron* of the family Ada. The TE was
216 inserted into an intron of a Phox domain-encoding gene (Supplementary Figure S8). Phox homologous
217 domain proteins contribute to sorting membrane trafficking (Odorizzi *et al.*, 2000). A third potentially
218 adaptive insertion of a *Copia* Deimos TE was 229 bp upstream of a gene encoding a SNARE domain
219 protein and 286 bp upstream of a gene encoding a flavin amine oxidoreductase and located in a region
220 of selective sweep (Supplementary Figure S9). SNARE domains play a role in vesicular transport and
221 membrane fusion (Bonifacino & Glick, 2004). Additional strong candidates for adaptive TE insertions
222 affected genes encoding a second MFS transporter and an effector candidate (Supplementary Figures
223 9 and 10). We experimentally tested whether the TE insertions in proximity to genes could contribute
224 to higher levels of fungicide resistance. For this, we measured growth rates of the fungal isolates in
225 the presence or absence of an azole fungicide widely deployed against the pathogen. We found that

226 the insertion of TEs at three loci was positively associated with higher levels of fungicide resistance

227 suggesting TE-mediated adaptations (Supplementary Figure S12).

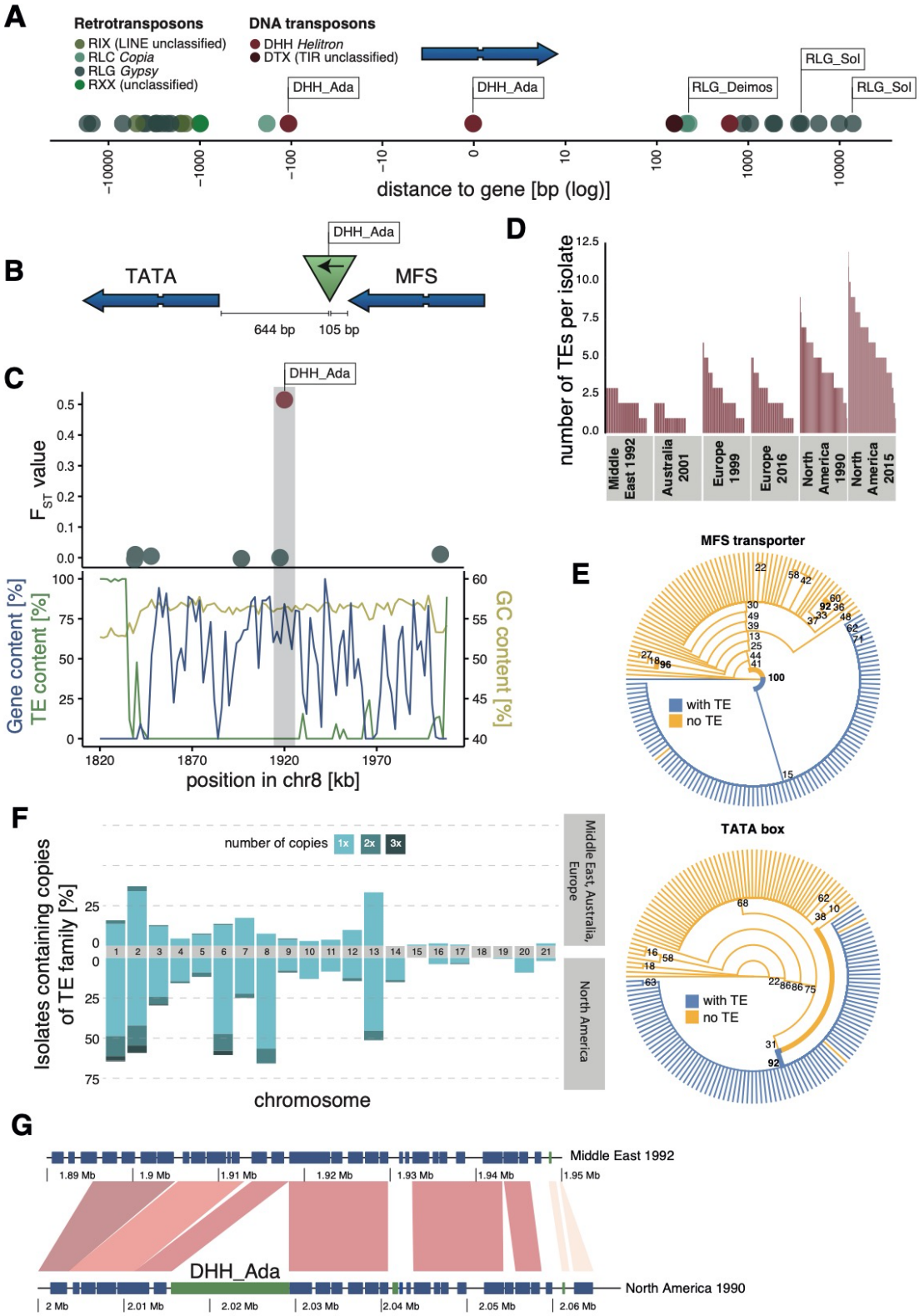

228

229 **Figure 4: Candidate adaptive transposable element (TE) insertions**. (A) Distribution of all extremely
230 differentiated TEs and their distance to the closest gene. Color indicates the superfamily. TE sites potentially
231 under selection according to F_{ST} are flagged. (B) Location of the *Helitron* Ada TE insertion on chromosome 8
232 corresponding to its two closest genes. (C) Genomic niche of the *Helitron* Ada TE insertion on chromosome 8:
233 F_{ST} values for each TE insertion, gene content (blue), TE content (green) and GC content (yellow). The grey
234 section highlights TE loci with extremely differentiated population frequencies. (D) Number of Ada copies per
235 isolate and population. (E) Phylogenetic trees of the coding sequences of each the MFS transporter upstream
236 and the TATA box downstream of the TE insertion. Isolates of the two North American populations and an
237 additional 11 isolates from other populations not carrying the insertion are shown. Blue color indicates TE
238 presence, yellow indicates TE absence. (F) Frequency changes of the TE family Ada between the two North
239 American populations compared to the other populations. Colors indicate the number of copies per chromosome.
240 (G) Synteny plot of the Ada insertion locus on chromosome 8 between two complete genomes from the Middle
241 East (TE missing) and North America (TE present). Figures S8-S11 show additional candidate regions.

242

243 POPULATION-LEVEL EXPANSIONS IN TE CONTENT

244 If TE insertion dynamics are largely neutral across populations, TE frequencies across loci should
245 reflect neutral population structure. To test this, we performed a principal component analysis based
246 on a set of six populations on four continents that represent the global genetic diversity of the pathogen
247 and 900'193 genome-wide SNPs (Figure 5A-B). The population structure reflected the demographic
248 history of the pathogen with clear continental differentiation and only minor within-site
249 differentiation. In stark contrast, TE frequencies across loci showed only weak clustering by
250 geographic origin with the Australian population being the most distinct (Figure 5D). We found a
251 surprisingly strong differentiation of the two North American populations sampled at a 25-year
252 interval in the same field in Oregon. To account for the lower number of TE loci, we performed an
253 additional principal component analysis using a comparably sized SNP set to number of TE loci.
254 Genome-wide SNPs retained the geographic signal of the broader set of SNPs (Figure 5C).

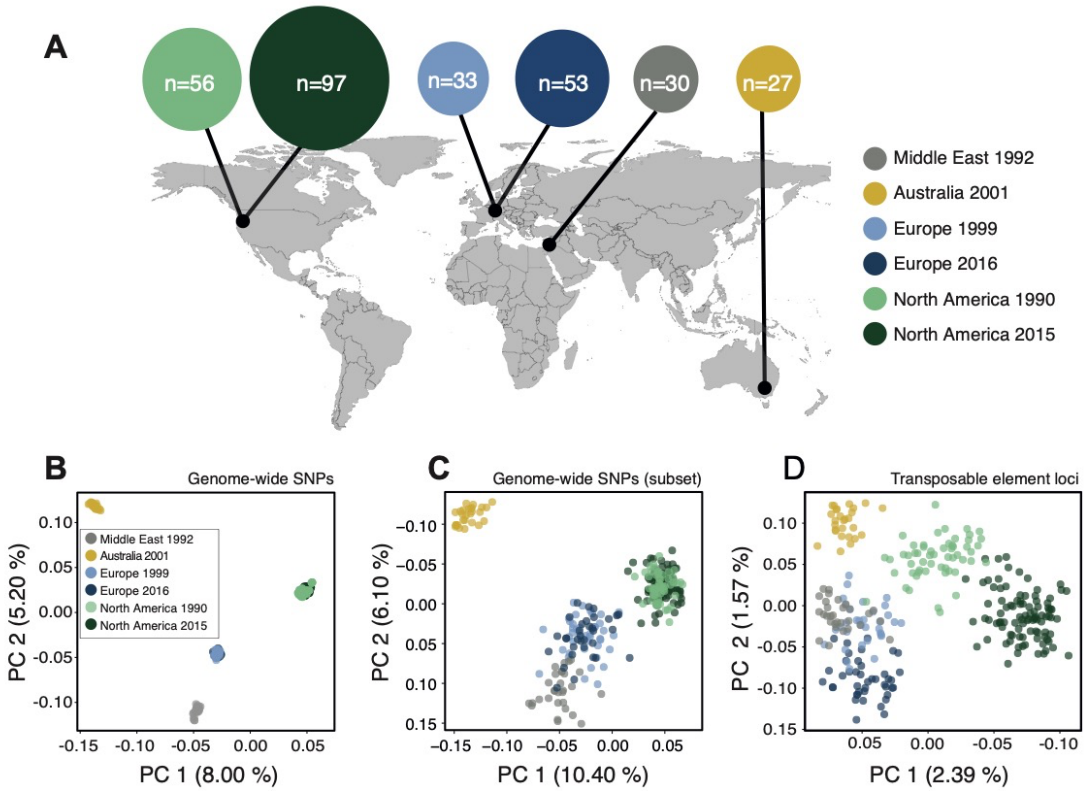

Figure 5: Population differentiation at transposable element (TE) and genome-wide SNP loci. (A) Sampling locations of the six populations. Middle East represents the region of origin of the pathogen. In North America, the two populations were collected at an interval of 25 years in the same field in Oregon. In Europe, two populations were collected at an interval of 17 years from two fields in Switzerland <20 km apart. Dark arrows indicate the historic colonization routes of the pathogen. (B) Principal component analysis (PCA) of 284 *Zymoseptoria tritici* isolates, based on 900'193 genome-wide SNPs. (C) PCA of a reduced SNP data set with randomly selected 203 SNPs matching approximately the number of analyzed TE loci. (D) PCA based on 193 TE insertion loci. Loci with allele frequency < 5% are excluded.

Unusual patterns in population differentiation at TE loci suggests that TE activity may substantially vary across populations (Figure 6). To analyze this, we first identified the total TE content across all loci per isolate. We found generally lower TE numbers in the Middle Eastern population from Israel (Figure 6B), which is close to the pathogen's center of origin (Stukenbrock *et al.*, 2007). Populations that underwent at least one migration bottleneck showed a substantial burst of TEs across all major superfamilies. These populations included the two populations from Europe collected in 1999 and 2016 and the North American population from 1990, as well as the Australian population. We found a second stark increase in TE content in the North American population sampled in 2015 at the same site as the population from 1990. Strikingly, the isolate with the lowest number of analyzed TEs collected in 2015 was comparable to the isolate with the highest number of TEs at the same site in

275 1990. We tested whether sequencing coverage could explain variation in the detected TEs across
276 isolates, but we found no meaningful association (Supplementary Figure S4B). We analyzed variation
277 in TE copy numbers across families and found that the expansions were mostly driven by *Gypsy*
278 elements including the families Luna, Sol and Venus, the *Copia* family Deimos and the LINE family
279 Lucy (Figure 6C; Supplementary Figures S5-6). We also found a North American specific burst in
280 *Helitron* elements (Ada), an increase specific to Swiss populations in LINE elements, and an increase
281 in *Copia* elements in the Australian and the two North American populations. Analyses of complete
282 *Z. tritici* genomes from the same populations revealed high TE contents in Australia and North
283 America (Oregon 1990) (Badet *et al.*, 2020). The complete genomes confirmed also that the increase
284 in TEs was driven by LINE, *Gypsy* and *Copia* families in Australia and *Helitron*, *Gypsy* and *Copia*
285 families in North America (Badet *et al.*, 2020).

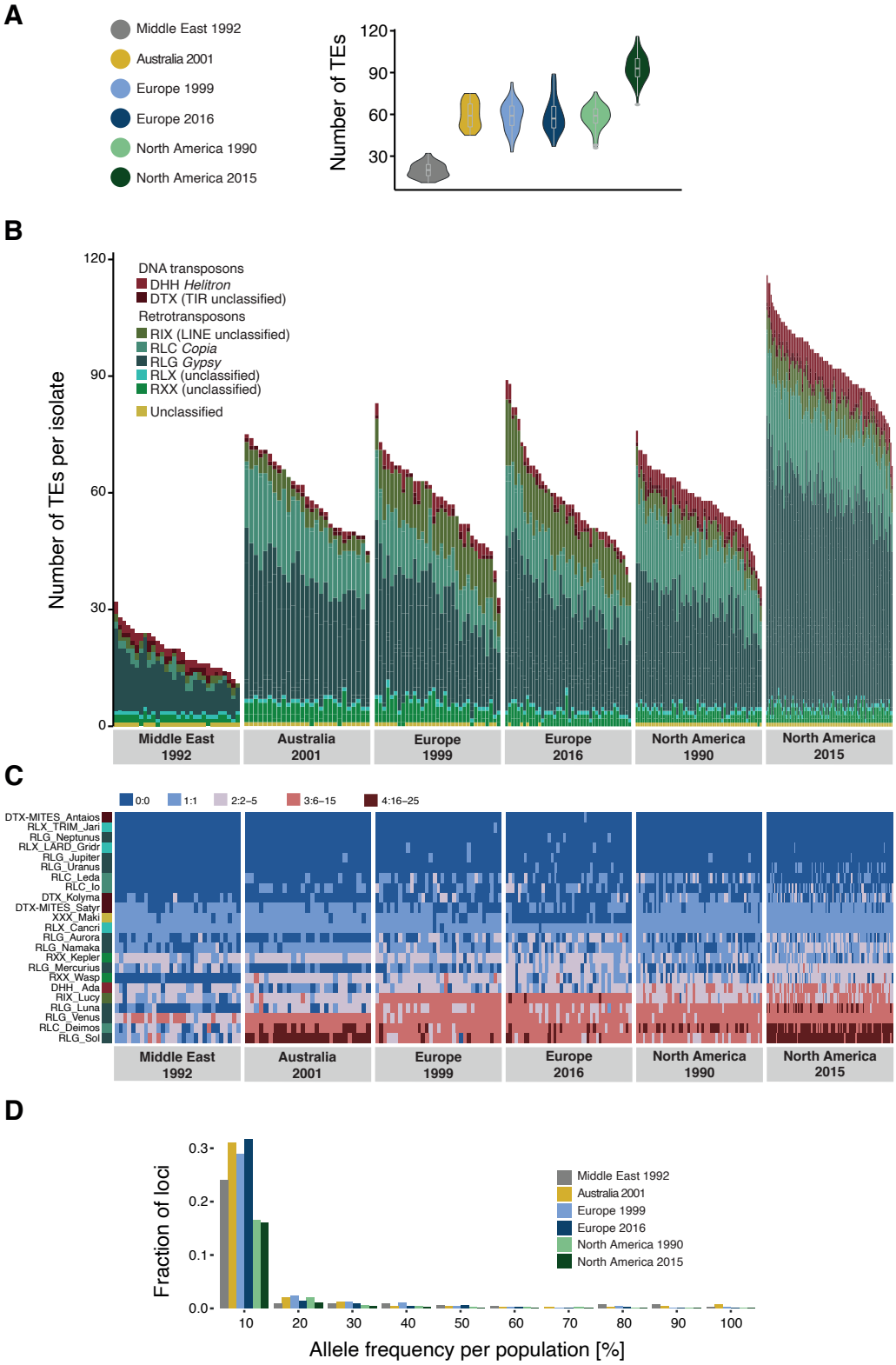

Figure 6: Global population structure of transposable element (TE) insertion polymorphism. (A) The number of transposable elements (TEs) per population. (B) Total TE copies per isolate. Colors identify TE superfamilies. (C) TE family copy numbers per isolate. (D) TE insertion frequency spectrum per population.

291 Finally, we analyzed whether the population-specific expansions were correlated with shifts in the
292 frequency spectrum of TEs in the populations (Figure 6D). We found that the first step of expansions
293 observed in Europe was associated with a downwards shift in allele frequencies. This is consistent
294 with transposition activity creating new copies in the genomes and stronger purifying selection. In
295 contrast, the North American populations showed an upwards shift in allele frequencies indicating
296 relaxation of selection against TEs.
297

298 TE-MEDIATED GENOME SIZE EXPANSIONS

299 The combined effects of actively copying TE families and relaxed purifying selection leads to an
300 accumulation of new TE insertions in populations. As a consequence, mean genome sizes in
301 populations should increase over generations. To test for incipient genome expansions within the
302 species, we first assembled genomes of all 284 isolates included in the study. Given the limitations of
303 short-read assemblies, we implemented corrective measures to compensate for potential variation in
304 assembly qualities. We corrected for variation in the GC content of different sequencing datasets by
305 downsampling reads to generate balanced sequencing read sets prior to assembly (see Methods). We
306 also excluded all reads mapping to accessory chromosomes because different isolates are known to
307 differ in the number of these chromosomes. Genome assemblies were checked for completeness by
308 retrieving the phylogenetically conserved BUSCO genes (Figure 7A). Genome assemblies across
309 different populations carry generally >99% complete BUSCO gene sets, matching the completeness
310 of fully finished genomes of the same species (Badet *et al.*, 2020). The completeness of the assemblies
311 showed no correlation with either TE or GC content of the genomes. GC content was inversely
312 correlated with genome size consistent with the expansion of repetitive regions having generally low
313 GC content (Figure 7B). We found that the core genome size varied substantially among populations
314 with the Middle East, Australia as well as the two older European and North American populations
315 having the smallest genomes (Figure 7C and 7D). We found a notable increase in genome size in both
316 the more recent European and North American populations. The increase in genome size is positively
317 correlated with the count of TE insertions (Figure 7E and G) and negatively correlated with the

genome-wide GC content (Figure 7F and G). Hence, genome size shows substantial variation within the species matching the recent expansion in TEs across continents.

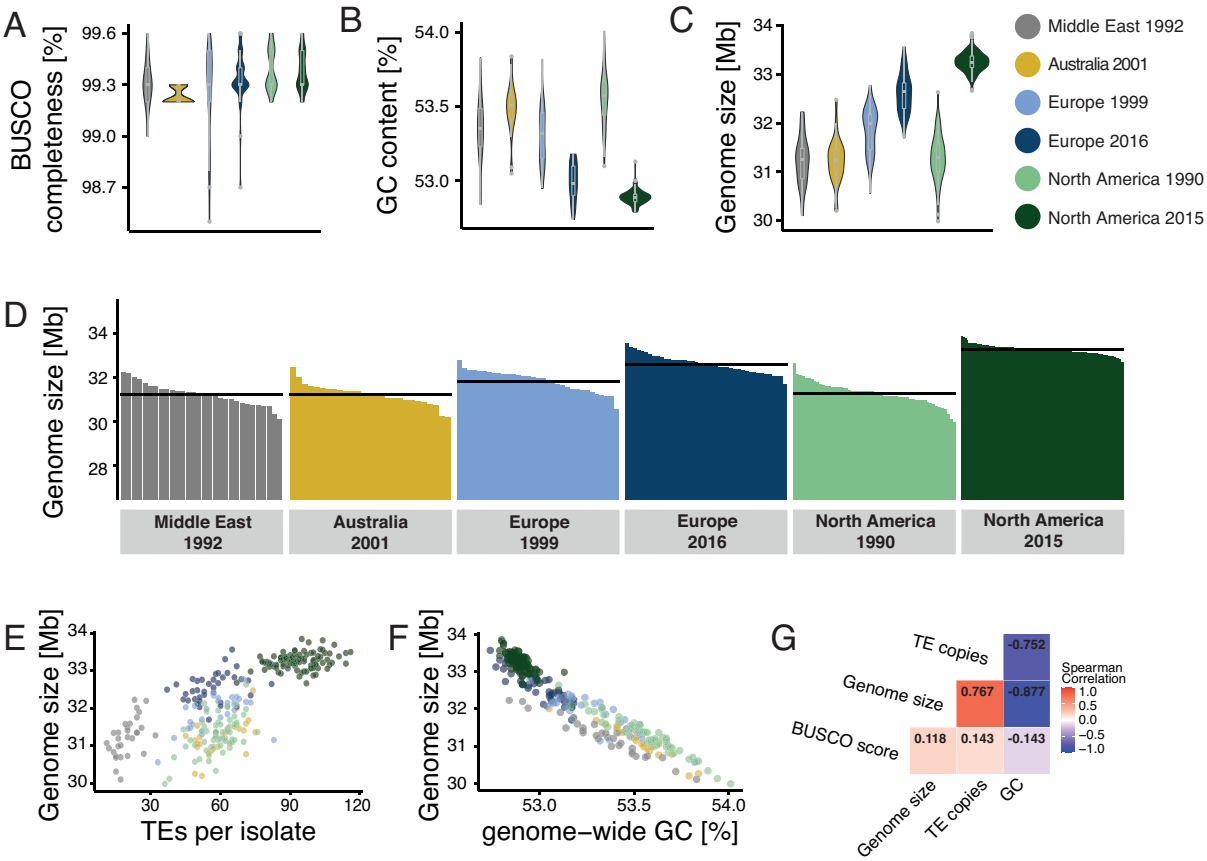

Figure 7: Genome size and transposable element (TE) evolution across populations. (A) BUSCO completeness variation among genome assemblies. Black lines indicate the mean genome size per population. (B) Genome-wide GC content variation. (C) Core genome sizes (excluding accessory chromosomes). (D) Genome size variation among population. (E) Correlation of core genome size and number of detected TEs. (F) Correlation of core genome size and genome-wide GC content. (G) Spearman correlation matrix of BUSCO completeness, core genome size, number of detected TEs and genome-wide GC content.

Discussion

TEs play a crucial role in generating adaptive genetic variation within species but are also drivers of deleterious genome expansions. We analyzed the interplay of TEs with selective and neutral processes including population differentiation and incipient genome expansions. TEs have substantial transposition activity in the genome but are strongly counter-selected and are maintained at low frequency. TE dynamics showed distinct trajectories across populations with more recently established populations having higher TE content and a concurrent expansion of the genome.

336

337 RECENT SELECTION ACTING ON TE INSERTIONS

338 TE frequencies in the species show a strong skew towards singleton insertions across populations.
339 This indicates both that TEs are undergoing transposition and that purifying selection maintains
340 frequencies at a low level. Similar effects of selection on active TEs were observed across plants and
341 animals, including *Drosophila melanogaster* and *Brachypodium distachyon* (Cridland *et al.*, 2013;
342 Stritt *et al.*, 2017; Luo *et al.*, 2020). TE insertions were under-represented in or near coding regions,
343 showing a stronger purifying selection against TEs inserting into genes. Coding sequences in the *Z.*
344 *tritici* genome are densely packed with an average distance of only ~1 kb (Goodwin *et al.*, 2011).
345 Consistent with this high gene density, TE insertions were most frequent at a distance of 200-400 bp
346 away from coding sequences. A rapid decay in linkage disequilibrium in the *Z. tritici* populations
347 (Croll *et al.*, 2015; Hartmann *et al.*, 2018) likely contributed to the efficiency of removing deleterious
348 insertions. We also found evidence for positive selection acting on TEs with the strongest candidate
349 loci being two TE insertions near genes encoding MFS transporters. Both loci showed a frequency
350 increase only in the North American populations, which experienced the first systematic fungicide
351 applications and subsequent emergence of fungicide resistance in the decade prior to the last sampling
352 (Estep *et al.*, 2015). TE-mediated overexpression of a MFS1 transporter is a known resistance
353 mechanism of *Z. tritici* and acts by increasing efflux of fungicides out of the cell (Omrane *et al.*, 2017).
354 TE-mediated fungicide resistance adaptation in the North American population is further supported
355 by a significant association of levels of fungicide resistance in the population and the presence of the
356 *Gypsy* insertion near the MFS gene. Furthermore, the locus experienced a selective sweep following
357 the insertion of the TE.

358 Transposition activity in a genome and counter-acting purifying selection are expected to establish an
359 equilibrium over evolutionary time (Charlesworth & Charlesworth, 1983). However, temporal bursts
360 of TE families and changes in population size due to bottlenecks or founder events are likely to shift
361 the equilibrium. Despite purifying selection, we were able to detect signatures of positive selection by
362 scanning for short-term population frequency shifts. Population genomic datasets can be used to
363 identify the most likely candidate loci underlying recent adaptation. The shallow genome-wide

364 differentiation of *Z. tritici* populations provides a powerful background to test for outlier loci
365 (Hartmann *et al.*, 2018). We found the same TE families to have experienced genome-wide copy
366 number expansions, suggesting that the availability of adaptive TE insertions may be a by-product of
367 TE bursts in individual populations.
368

369 POPULATION-LEVEL TE INVASIONS AND RELAXED SELECTION

370 Across the surveyed populations from four continents, we identified substantial variation in TE counts
371 per genome. The increase in TEs matches the global colonization history of the pathogen with an
372 increase in TE copies in more recently established populations (Zhan *et al.*, 2003; Stukenbrock *et al.*,
373 2007). Compared to the Israeli population located nearest the center of origin in the Middle East, the
374 European populations showed a three-fold increase in TE counts. The Australian and North American
375 populations established from European descendants retained high TE counts. We identified a second
376 increase at the North American site where TE counts nearly doubled again over a 25-year period.
377 Compared to the broader increase in TEs from the Middle East, the second expansion at the North
378 American site was driven by a small subset of TE families alone. Analyses of completely assembled
379 genomes from the same populations confirmed that genome expansions were primarily driven by the
380 same TE families belonging to *Gypsy*, *Copia* and *Helitron* superfamilies (Badet *et al.*, 2020).
381 Consistent with the contributions from individual TEs, we found that the first expansion in Europe led
382 to an increase in low-frequency variants, suggesting higher transposition activity of many TEs in
383 conjunction with strong purifying selection. The second expansion at the North American site shifted
384 TE frequencies upwards, suggesting relaxed selection against TEs. The population-level context of
385 TEs in *Z. tritici* shows how heterogeneity in TE control interacts with demography to determine extant
386 levels of TE content and, ultimately, genome size.
387

388 TE INVASION DYNAMICS UNDERPINS GENOME SIZE EXPANSIONS

389 The number of detected TEs was closely correlated with core genome size, hence genome size
390 expansions were at least partly caused by the very recent proliferation of TEs. Genome assemblies of
391 large eukaryotic genomes based on short read sequencing are often fragmented and contain chimeric

392 sequences (Nagarajan & Pop, 2013). Focusing on the less repetitive core chromosomes in the genome
393 of *Z. tritici* reduces such artefacts substantially. Because genome assemblies are the least complete in
394 the most repetitive regions, any underrepresented sequences may rather underestimate than
395 overestimate within-species variation in genome size. Hence, we consider the assembly sizes to be a
396 robust correlate of total genome size. The core genome size differences observed across the species
397 range match genome size variation typically observed among closely related species. Among primates,
398 genome size varies by ~70% with ~10% between humans and chimpanzees (Rogers & Gibbs, 2014;
399 Miga *et al.*, 2020). In fungi, genome size varies by several orders of magnitude within phyla but is
400 often highly similar among closely related species (Raffaele & Kamoun, 2012). Interestingly, drastic
401 changes in genome size have been observed in the *Blumeria* and *Pseudocercospora* genera where
402 genome size changed by 35-130% between the closest known species (González-Sayer *et al.*;
403 Frantzeskakis *et al.*, 2018). Beyond analyses of TE content variation correlating with genome size
404 evolution, proximate mechanisms driving genome expansions are poorly understood. Establishing
405 large population genetic datasets such as it is possible for crop pathogens, genome size evolution
406 becomes tractable at the population level.
407 The activity of TEs is controlled by complex selection regimes within species. Actively transposing
408 elements may accelerate genome evolution and underpin expansions. Hence, genomic defenses should
409 evolve to efficiently target recently active TEs. Here, we show that TE activity and counteracting
410 genomic defenses have established a tenuous equilibrium across the species range. We show that
411 population subdivisions are at the origin of highly differentiated TE content within a species matching
412 genome size changes emerging over the span of only decades and centuries. In conclusion, population-
413 level analyses of genome size can recapitulate genome expansions typically observed across much
414 deeper time scales providing fundamentally new insights into genome evolution.
415

416 # METHODS

417 ## FUNGAL ISOLATE COLLECTION AND SEQUENCING

418 We analyzed 295 *Z. tritici* isolates covering six populations originating from four geographic locations
419 and four continents (Supplementary Table S1), including: Middle East 1992 (*n* = 30 isolates, Nahal
420 Oz, Israel), Australia 2001 (*n* = 27, Wagga Wagga), Europe 1999 (*n* = 33, Berg am Irchel,
421 Switzerland), Europe 2016 (*n* = 52, Eschikon, ca. 15km from Berg am Irchel, Switzerland), North
422 America 1990 and 2015 (*n* = 56 and *n* = 97, Willamette Valley, Oregon, United States) (McDonald *et*
423 *al.*, 1996; Linde *et al.*, 2002; Zhan *et al.*, 2002, 2003, 2005). Illumina short read data from the Middle
424 East, Australia, European 1999 and North American 1990 populations were obtained from the NCBI
425 Short Read Archive under the BioProject PRJNA327615 (Hartmann *et al.*, 2017). For, the Switzerland
426 2016 and Oregon 2015 populations, asexual spores were harvested from infected wheat leaves from
427 naturally infected fields and grown in YSB liquid media including 50 mgL^{-1} kanamycin and stored in
428 silica gel at −80°C. High-quality genomic DNA was extracted from liquid cultures using the DNeasy
429 Plant Mini Kit from Qiagen (Venlo, Netherlands). The isolates were sequenced on an Illumina HiSeq
430 in paired-end mode and raw reads were deposited on the NCBI Short Read Archive under the
431 BioProject PRJNA596434.

432

433 ## TE INSERTION DETECTION

434 The quality of Illumina short reads was determined with FastQC version 0.11.5
435 (https://www.bioinformatics.babraham.ac.uk/projects/fastqc/) (Figure 1A). To remove spuriously
436 sequenced Illumina adaptors and low quality reads, we trimmed the sequences with Trimmomatic
437 version 0.36, using the following filter parameters: illuminaclip:TruSeq3-PE-2.fa:2:30:10 leading:10
438 trailing:10 slidingwindow:5:10 minlen:50 (Bolger *et al.*, 2014). We created repeat consensus
439 sequences for TE families (sequences are available on https://github.com/crolllab/datasets) in the
440 complete reference genome IPO323 (Goodwin *et al.*, 2011) with RepeatModeler version open-4.0.7
441 (http://www.repeatmasker.org/RepeatModeler/) based on the RepBase Sequence Database and de
442 novo (Bao *et al.*, 2015). TE classification into superfamilies and families was based on an approach

443 combining detection of conserved protein sequences and tools to detect non-autonomous TEs (Badet
444 *et al.*, 2020). To detect TE insertions, we used the R-based tool ngs_te_mapper version
445 79ef861f1d52cdd08eb2d51f145223fad0b2363c integrated into the McClintock pipeline version
446 20cb912497394fabddcdaa175402adacf5130bd1, using bwa version 0.7.4-r385 to map Illumina short
447 reads, samtools version 0.1.19 to convert alignment file formats and R version 3.2.3 (Li & Durbin,
448 2009; Li *et al.*, 2009; Linheiro & Bergman, 2012; R Core Team, 2017; Nelson *et al.*, 2017).
449

450 DOWN-SAMPLING ANALYSIS

451 We performed a down-sampling analysis to estimate the sensitivity of the TE detection with
452 ngs_te_mapper based on variation in read depth. We selected one isolate per population matching the
453 average coverage of the population. We extracted the per-base pair read depth with the genomecov
454 function of bedtools version 2.27.1 and calculated the genome-wide mean read depth (Quinlan & Hall,
455 2010). The number of reads in the original fastq file was reduced in steps of 10% to simulate the
456 impact of reduced coverage. We analyzed each of the obtained reduced read subsets with
457 ngs_te_mapper using the same parameters as described above. The correlation between the number of
458 detected insertions and the read depth was visualized using the function nls with model SSlogis in R
459 and visualized with ggplot2 (Wickham, 2016). The number of detected TEs increased with the number
460 of reads until reaching a plateau indicating saturation (Figure 1B). Saturation was reached at a
461 coverage of approximately 15X, hence we retained only isolates with an average read depth above
462 15X for further analyses. We thus excluded one isolate from the Oregon 2015 population and ten
463 isolates from the Switzerland 2016 population.
464

465 VALIDATION PROCEDURE FOR PREDICTED TE INSERTIONS

466 ngs_te_mapper detects the presence but not the absence of a TE at any given locus. We devised
467 additional validation steps to ascertain both the presence as well as the absence of a TE across all loci
468 in all individuals. TEs absent in the reference genome were validated by re-analyzing mapped Illumina
469 reads. Reads spanning both parts of a TE sequence and an adjacent chromosomal sequence should

470 only map to the reference genome sequence and cover the target site duplication (TSD) of the TE
471 (Figure 1C). We used bowtie2 version 2.3.0 with the parameter --very-sensitive-local to map Illumina
472 short reads of each isolate on the reference genome IPO323 (Langmead & Salzberg, 2012). Mapped
473 Illumina short reads were then sorted and indexed with samtools and the resulting bam file was
474 converted to a bed file with the function bamtobed in bedtools. We extracted all mapped reads with
475 an end point located within 100 bp of the TSD (Figure 1C). We tested whether the number of reads
476 with a mapped end around the TSD significantly deviated if the mapping ended exactly at the
477 boundary. A mapped read ending exactly at the TSD boundary is indicative of a split read mapping to
478 a TE sequence not present in the reference genome. To test for the deviation in the number of read
479 mappings around the TSD, we used a Poisson distribution and the *ppois* function in R version 3.5.1
480 (Figure 1C). We identified a TE as present in an isolate if tests on either side of the TSD had a *p*-value
481 < 0.001 (Supplementary Table S1, S2, Figure S1B).
482
483 For TEs present in the reference genome, we analyzed evidence for spliced junction reads spanning
484 the region containing the TE. Spliced reads are indicative of a discontinuous sequence and, hence,
485 absence of the TE in a particular isolate (Figure 1D). We used STAR version 2.5.3a to detect spliced
486 junction reads with the following set of parameters: --runThreadN 1 --outFilterMultimapNmax 100 -
487 -winAnchorMultimapNmax 200 --outSAMmultNmax 100 --outSAMtype BAM Unsorted --
488 outFilterMismatchNmax 5 --alignIntronMin 150 --alignIntronMax 15000 (Dobin *et al.*, 2012). We
489 then sorted and indexed the resulting bam file with samtools and converted split junction reads with
490 the function bam2hints in bamtools version 2.5.1 (Barnett *et al.*, 2011). We selected loci without
491 overlapping spliced junction reads using the function intersect in bedtools with the parameter -loj -v.
492 We considered a TE as truly absent in an isolate if ngs_te_mapper did not detect a TE and evidence
493 for spliced junction reads were found. If the absence of a TE could not be confirmed by spliced
494 junction reads, we labelled the genotype as missing. Finally, we excluded TE loci with more than 20%
495 missing data from further investigations (Figure 1D and Supplementary Figure S1C).
496

497 CLUSTERING OF TE INSERTIONS INTO LOCI

498 We identified insertions across isolates as being the same locus if all detected TEs belonged to the
499 same TE family and insertion sites differed by ≤100 bp (Supplementary Figure S2). We used the R
500 package *GenomicRanges* version 1.28.6 with the functions makeGRangesFromDataFrame and
501 findOverlaps and the R package *devtools* version 1.13.4 (Lawrence *et al.*, 2013; Wickham & Chang,
502 2016). We used the R package *dplyr* version 0.7.4 to summarize datasets (https://dplyr.tidyverse.org/).
503 Population-specific frequencies of insertions were calculated with the function allele.count in the R
504 package *hierfstat* version 0.4.22 (Goudet, 2005). We conducted a principal component analysis for TE
505 insertion frequencies filtering for a minor allele frequency ≥ 5%. We also performed a principal
506 component analysis for genome-wide single nucleotide polymorphism (SNP) data obtained from
507 Hartmann et al (2017). As described previously, SNPs were hard-filtered with VariantFiltration and
508 SelectVariants tools integrated in the Genome Analysis Toolkit (GATK) (McKenna *et al.*, 2010).
509 SNPs were removed if any of the following filter conditions applied: QUAL<250; QD<20.0;
510 MQ<30.0; -2 > BaseQRankSum > 2; -2 > MQRankSum > 2; -2 > ReadPosRankSum > 2; FS>0.1.
511 SNPs were excluded with vcftools version 0.1.17 and plink version 1.9 requiring a genotyping rate
512 >90% and a minor allele frequency >5% (https://www.cog-genomics.org/plink2, Chang et al., 2015).
513 Finally, we converted tri-allelic SNPs to bi-allelic SNPs by recoding the least frequent allele as a
514 missing genotype. Principal component analysis was performed using the *gdsfmt* and *SNPRelate*
515 packages in R (Zheng *et al.*, 2012, 2017). For a second principal component analysis with a reduced
516 set of random markers, we randomly selected SNPs with vcftools and the following set of parameters:
517 --maf 0.05 –thin 200'000 to obtain an approximately equivalent number of SNPs as TE loci.

518

519 GENOMIC LOCATION OF TE INSERTIONS

520 To characterize the genomic environment of TE insertion loci, we split the reference genome into non-
521 overlapping windows of 10 kb using the function splitter from EMBOSS version 6.6.0 (Rice *et al.*,
522 2000). TEs were located in the reference genome using RepeatMasker providing consensus sequences
523 from RepeatModeler (http://www.repeatmasker.org/). To analyze coding sequence, we retrieved

524 the gene annotation for the reference genome (Grandaubert *et al.*, 2015). We estimated the percentage
525 covered by genes or TEs per window using the function intersect in bedtools. Additionally, we
526 calculated the GC content using the tool get_gc_content (https://github.com/spundhir/RNA-
527 Seq/blob/master/get_gc_content.pl). We also extracted the number of TEs present in 1 kb windows
528 up- and downstream of each annotated gene with the function window in bedtools with the parameters
529 -l 1000 -r 1000 and calculated the relative distances with the closest function in bedtools. For the TEs
530 inserted into genes, we used the intersect function in bedtools to distinguish intron and exon insertions
531 with the parameters -wo and -v, respectively. For each 100 bp segment in the 1kb windows as well as
532 for introns and exons, we calculated the mean number of observed TE insertions per base pair.
533

534 POPULATION DIFFERENTIATION IN TE FREQUENCIES

535 We calculated Nei's fixation index (F_{ST}) between pairs of populations using the R packages *hierfstat*
536 and *adegenet* version 2.1.0 (Jombart, 2008; Jombart & Ahmed, 2011). To understand the chromosomal
537 context of TE insertion loci across isolates, we analyzed draft genome assemblies. We generated *de*
538 *novo* genome assemblies for all isolates using SPAdes version 3.5.0 with the parameter --careful and
539 a kmer range of "21, 29, 37, 45, 53, 61, 79, 87" (Bankevich *et al.*, 2012). We used blastn to locate
540 genes adjacent to TE insertion loci on genomic scaffolds of each isolate. We then extracted scaffold
541 sequences surrounding 10 kb up- and downstream of the localized gene with the function faidx in
542 samtools and reverse complemented the sequence if needed. Then, we performed multiple sequence
543 alignments for each locus across all isolates with MAFFT version 7.407 with parameter --maxiterate
544 1000 (Katoh & Standley, 2013). We performed visual inspections to ensure correct alignments across
545 isolates using Jalview version 2.10.5 (Waterhouse *et al.*, 2009). To generate phylogenetic trees of
546 individual gene or TE loci, we extracted specific sections of the alignment using the function
547 extractalign in EMBOSS and converted the multiple sequence alignment into PHYLIP format with
548 jmodeltest version 2.1.10 using the -getPhylip parameter. We then estimated maximum likelihood
549 phylogenetic trees with the software PhyML version 3.0, the K80 substitution model and 100
550 bootstraps on the ATGC South of France bioinformatics platform (Guindon & Gascuel, 2003;
551 Guindon *et al.*, 2010; Darriba *et al.*, 2012). Bifurcations with a supporting value lower than 10% were

552 collapsed in TreeGraph version 2.15.0-887 beta and trees were visualized as circular phylograms in
553 Dendroscope version 2.7.4 (Huson *et al.*, 2007; Stöver & Müller, 2010). For loci showing complex
554 rearrangements, we generated synteny plots using 19 completely sequenced genomes from the same
555 species using the R package *genoplotR* version 0.8.9 (Guy *et al.*, 2010; Badet *et al.*, 2020).
556 We analyzed signatures of selective sweeps using the extended haplotype homozygosity (EHH) tests
557 (Sabeti *et al.*, 2007) implemented in the R package REHH (Gautier & Vitalis, 2012). We analyzed
558 within-population signatures based on the iHS statistic and chose a maximum gap distance of 20 kb.
559 We also analyzed cross-population EHH (XP-EHH) signatures testing the following two population
560 pairs: North America 1990 versus North America 2015, Europe 1999 versus Europe 2016. We defined
561 significant selective sweeps as being among the 99.9th percentile outliers of the iHS and XP-EHH
562 statistics. Significant SNPs at less than 5 kb were clustered into a single selective sweep region adding
563 +/- 2.5 kb. Finally, we analyzed whether TE loci were within 10 kb of a region identified as a selective
564 sweep using the function intersect from bedtools.

565

566 GENOME SIZE ESTIMATION

567 Accessory chromosomes show presence/absence variation within the species and length
568 polymorphism (Goodwin *et al.*, 2011; Croll *et al.*, 2013) and thus impact genome size. We controlled
569 for this effect by first mapping sequencing reads to the reference genome IPO323 using bowtie2 with
570 --very-sensitive-local settings and retained only reads mapping to any of the 13 core chromosomes
571 using seqtk subseq v1.3-r106 (https://github.com/lh3/seqtk/). Furthermore, we found that different
572 sequencing runs showed minor variation in the distribution of the per read GC content. In particular,
573 reads of a GC content lower than 30 % were underrepresented in the Australian (mean reads < 30 %
574 of the total readset: 0.05 %), North American 1990 (0.07 %) and Middle East (0.1 %) populations, and
575 higher in the Europe 1999 (1.3 %), North American 2015 (3.0 %) and Europe 2016 (4.02 %)
576 populations (Supplementary Figure S3). Library preparation protocols and Illumina sequencer
577 generations are known factors influencing the recovery of reads of varying GC content (Benjamini &
578 Speed, 2012).

579

580 To control a potential bias stemming from this, we subsampled reads based on GC content to create
581 homogeneous datasets. For this, we first retrieved the mean GC content for each read pair using geecee
582 in EMBOSS and binned reads according to GC content. For the bins with a GC content <30%, we
583 calculated the mean proportion of reads from the genome over all samples. We then used seqtk subseq
584 to subsample reads of <30% to adjust the mean GC content among readsets. We generated *de novo*
585 genome assemblies using the SPAdes assembler version with the parameters --careful and a kmer
586 range of "21, 29, 37, 45, 53, 61, 79, 87". The SPAdes assembler is optimized for the assembly of
587 relatively small eukaryotic genomes. We evaluated the completeness of the assemblies using BUSCO
588 v4.1.1 with the fungi_odb10 gene test set (Simão *et al.*, 2015). We finally ran Quast v5.0.2 to retrieve
589 assembly metrics including scaffolds of at least 1kb (Mikheenko *et al.*, 2018).

590

591 FUNGICIDE RESISTANCE ASSAY

592 To quantify susceptibility towards propiconazole we performed a microtiter plate assay. Isolates were
593 grown on yeast malt sucrose agar for five days and spores were harvested. We then tested for growth
594 inhibition by growing spores (2.5 x 10^4 spores/ml) in Sabouraud-dextrose liquid medium with
595 differing concentrations of propiconazole (0.00006, 0.00017, 0.0051, 0.0086, 0.015, 0.025, 0.042,
596 0.072, 0.20, 0.55, 1.5 mg/L). We incubated the plates stationary in the dark at 21°C and 80% relative
597 humidity for four days and measured optical density at 605 nm. We calculated EC_{50} with the R package
598 *drc* (Ritz & Streibig, 2005).

599

600 **Data availability**

601 Sequence data is deposited on the NCBI Short Read Archive under the accession numbers
602 PRJNA327615, PRJNA596434 and PRJNA178194. Transposable element consensus sequences are
603 available from https://github.com/crolllab/datasets.

604

605 **Author contributions**

UO and DC conceived the study, UO, TW and DC designed analyses, UO, TB, TV and FEH performed analyses, FEH, NKS, LNA, PK, CCM and BAM provided samples/datasets, BAM and DC provided funding, UO and DC wrote the manuscript with input from co-authors. All authors reviewed the manuscript and agreed on submission.

Acknowledgments

We thank Andrea Sánchez Vallet, Anne C. Roulin, Luzia Stalder, Adam Taranto, Emilie Chanclud and Alice Feurtey for helpful discussions and comments on previous versions of the manuscript. DC is supported by the Swiss National Science (grants 31003A_173265 and IZCOZO_177052) and the Fondation Pierre Mercier pour la Science.

Competing interests

We declare to have no competing interests.

REFERENCES

Badet T, Oggenfuss U, Abraham L, McDonald BA, Croll D. **2020**. A 19-isolate reference-quality global pangenome for the fungal wheat pathogen Zymoseptoria tritici. *BMC Biology* **18**: 12.

Bankevich A, Nurk S, Antipov D, Gurevich AA, Dvorkin M, Kulikov AS, Lesin VM, Nikolenko SI, Pham S, Prjibelski AD, *et al.* 2012. SPAdes: a new genome assembly algorithm and its applications to single-cell sequencing. *Journal of computational biology : a journal of computational molecular cell biology* **19**: 455–77.

Bao W, Kojima KK, Kohany O. **2015**. Repbase Update, a database of repetitive elements in eukaryotic genomes. *Mobile DNA* **6**: 4–9.

Barnett DW, Garrison EK, Quinlan AR, Stŕmberg MP, Marth GT. **2011**. Bamtools: A C++ API and toolkit for analyzing and managing BAM files. *Bioinformatics* **27**: 1691–1692.

Baucom RS, Estill JC, Leebens-Mack J, Bennetzen JL. **2008**. Natural selection on gene function drives the evolution of LTR retrotransposon families in the rice genome. *Genome Research* **19**: 243–254.

Benjamini Y, Speed TP. **2012**. Summarizing and correcting the GC content bias in high-throughput sequencing. *Nucleic Acids Research* **40**: 1–14.

Bolger AM, Lohse M, Usadel B. **2014**. Trimmomatic: a flexible trimmer for Illumina sequence data.

Bioinformatics **30**: 2114–2120.

Bonifacino JS, Glick BS. **2004**. The Mechanisms of Vesicle Budding and Fusion. *Cell* **116**: 153–166.

Charlesworth B, Charlesworth D. **1983**. The population dynamics of transposable elements. *Genetical Research* **42**: 1–27.

Chuong EB, Elde NC, Feschotte C. **2017**. Regulatory activities of transposable elements: from conflicts to benefits. *Nature Reviews Genetics* **18**: 71–86.

Cridland JM, Macdonald SJ, Long AD, Thornton KR. **2013**. Abundance and distribution of transposable elements in two drosophila QTL mapping resources. *Molecular Biology and Evolution* **30**: 2311–2327.

Croll D, Lendenmann MH, Stewart E, McDonald BA. **2015**. The Impact of Recombination Hotspots on Genome Evolution of a Fungal Plant Pathogen. *Genetics* **201**: 1213-U787.

Croll D, Zala M, McDonald BA. **2013**. Breakage-fusion-bridge Cycles and Large Insertions Contribute to the Rapid Evolution of Accessory Chromosomes in a Fungal Pathogen (J Heitman, Ed.). *PLOS Genetics* **9**: e1003567.

Darriba D, Taboada GL, Doallo R, Posada D. **2012**. jModelTest 2: more models, new heuristics and parallel computing. *Nature Methods* **9**: 772.

Dobin A, Davis CA, Schlesinger F, Drenkow J, Zaleski C, Jha S, Gingeras TR, Batut P, Chaisson M. **2012**. STAR: ultrafast universal RNA-seq aligner. *Bioinformatics* **29**: 15–21.

Eichler EE, Sankoff D. **2003**. Structural dynamics of eukaryotic chromosome evolution. *Science* **301**: 793–797.

Estep LK, Torriani SFF, Zala M, Anderson NP, Flowers MD, Mcdonald BA, Mundt CC, Brunner PC. **2015**. Emergence and early evolution of fungicide resistance in North American populations of Zymoseptoria tritici. *Plant Pathology* **64**: 961–971.

Feschotte C. **2008**. Transposable elements and the evolution of regulatory networks. *Nature Reviews Genetics* **9**: 397–405.

Feurtey A, Lorrain C, Croll D, Eschenbrenner C, Freitag M, Habig M, Haueisen J, Möller M, Schotanus K, Stukenbrock EH. **2020**. Genome compartmentalization predates species divergence in the plant pathogen genus Zymoseptoria. *BMC genomics* **21**: 588.

Fouché S, Badet T, Oggenfuss U, Plissonneau C, Francisco CS, Croll D. **2019**. Stress-driven transposable element de-repression dynamics in a fungal pathogen. *Molecular Biology and Evolution*.

Frantzeskakis L, Kracher B, Kusch S, Yoshikawa-Maekawa M, Bauer S, Pedersen C, Spanu PD, Maekawa T, Schulze-Lefert P, Panstruga R. **2018**. Signatures of host specialization and a recent transposable element burst in the dynamic one-speed genome of the fungal barley powdery mildew pathogen. *BMC Genomics* **19**: 1–23.

Gautier M, Vitalis R. **2012**. Rehh An R package to detect footprints of selection in genome-wide SNP data from haplotype structure. *Bioinformatics* **28**: 1176–1177.

González-Sayer S, Oggenfuss U, García I, Aristizabal F. High-quality genome assembly of Pseudocercospora ulei the main threat to natural rubber trees. : 0–1.

Goodwin SB, Ben M'Barek S, Dhillon B, Wittenberg AHJ, Crane CF, Hane JK, Foster AJ, Van der Lee TAJ, Grimwood J, Aerts A, *et al.* 2011. Finished Genome of the Fungal Wheat Pathogen Mycosphaerella graminicola Reveals Dispensome Structure, Chromosome Plasticity, and Stealth Pathogenesis (HS Malik, Ed.). *PLOS Genetics* **7**: e1002070.

Goudet J. **2005**. Hierstat, a package for R to compute and test heirarchical F-statistics. *Molecular*

683 *Ecology Notes* **5**: 184–186.

684 **Grandaubert J, Bhattacharyya A, Stukenbrock EH**. **2015**. RNA-seq-Based Gene Annotation and
685 Comparative Genomics of Four Fungal Grass Pathogens in the Genus Zymoseptoria Identify Novel
686 Orphan Genes and Species-Specific Invasions of Transposable Elements. *G3-Genes Genomes*
687 *Genetics* **5**: 1323–1333.

688 **Guindon S, Dufayard J-F, Lefort V, Anisimova M, Hordijk W, Gascuel O**. **2010**. New Algorithms
689 and Methods to Estimate Maximum-Likelihood Phylogenies: Assessing the Performance of
690 PhyML 3.0. *Systematic Biology* **59**: 307–321.

691 **Guindon S, Gascuel O**. **2003**. A simple, fast, and accurate algorithm to estimate large phylogenies
692 by maximum likelihood. *Systematic Biology* **52**: 696–704.

693 **Guy L, Kultima JR, Andersson SGE**. **2010**. GenoPlotR: comparative gene and genome visualization
694 in R. *Bioinformatics* **26**: 2334–2335.

695 **Hartmann F, Croll D**. **2017**. Distinct Trajectories of Massive Recent Gene Gains and Losses in
696 Populations of a Microbial Eukaryotic Pathogen. *Molecular Biology and Evolution*.

697 **Hartmann F, McDonald M, Croll D**. **2018**. Genome-wide evidence for divergent selection between
698 populations of a major agricultural pathogen. *Molecular Ecology* **27**: 2725–2741.

699 **Hartmann FE, Sánchez-Vallet A, McDonald BA, Croll D**. **2017**. A fungal wheat pathogen evolved
700 host specialization by extensive chromosomal rearrangements. *The ISME Journal* **11**: 1189–1204.

701 **Hollister JD, Gaut BS**. **2009**. Epigenetic silencing of transposable elements: A trade-off between
702 reduced transposition and deleterious effects on neighboring gene expression. *Genome Research*
703 **19**: 1419–1428.

704 **Huson DH, Richter DC, Rausch C, Dezulian T, Franz M, Rupp R**. **2007**. Dendroscope: An
705 interactive viewer for large phylogenetic trees. *BMC Bioinformatics* **8**: 1–6.

706 **Jiao W-B, Schneeberger K**. **2019**. Chromosome-level assemblies of multiple Arabidopsis thaliana
707 accessions reveal hotspots of genomic rearrangements. *bioRxiv*: 738880.

708 **Jombart T**. **2008**. Adegenet: A R package for the multivariate analysis of genetic markers.
709 *Bioinformatics* **24**: 1403–1405.

710 **Jombart T, Ahmed I**. **2011**. adegenet 1.3-1: New tools for the analysis of genome-wide SNP data.
711 *Bioinformatics* **27**: 3070–3071.

712 **Katoh K, Standley DM**. **2013**. MAFFT multiple sequence alignment software version 7:
713 Improvements in performance and usability. *Molecular Biology and Evolution* **30**: 772–780.

714 **Kidwell MG**. **2002**. Transposable elements and the evolution of genome size in eukaryotes. *Genetica*
715 **115**: 49–63.

716 **Krishnan P, Meile L, Plissonneau C, Ma X, Hartmann FE, Croll D, McDonald BA, Sánchez-**
717 **Vallet A**. **2018**. Transposable element insertions shape gene regulation and melanin production in
718 a fungal pathogen of wheat. *BMC Biology* **16**: 1–18.

719 **Lai X, Schnable JC, Liao Z, Xu J, Zhang G, Li C, Hu E, Rong T, Xu Y, Lu Y**. **2017**. Genome-
720 wide characterization of non-reference transposable element insertion polymorphisms reveals
721 genetic diversity in tropical and temperate maize. *BMC Genomics* **18**: 1–13.

722 **Langmead B, Salzberg SL**. **2012**. Fast gapped-read alignment with Bowtie 2. *Nature Methods* **9**:
723 357–359.

724 **Lawrence M, Huber W, Pagès H, Aboyoun P, Carlson M, Gentleman R, Morgan MT, Carey VJ**.
725 **2013**. Software for Computing and Annotating Genomic Ranges (A Prlic, Ed.). *PLOS*
726 *Computational Biology* **9**: e1003118.

Li H, Durbin R. **2009**. Fast and accurate short read alignment with Burrows-Wheeler transform. *Bioinformatics* **25**: 1754–1760.

Li H, Handsaker B, Wysoker A, Fennell T, Ruan J, Homer N, Marth G, Abecasis G, Durbin R. **2009**. The Sequence Alignment/Map format and SAMtools. *Bioinformatics* **25**: 2078–2079.

Lim JK. **1988**. Intrachromosomal rearrangements mediated by hobo transposons in Drosophila melanogaster. *PNAS* **85**: 9153–9157.

Linde CC, Zhan J, McDonald BA. **2002**. Population Structure of *Mycosphaerella graminicola* : From Lesions to Continents. *Phytopathology* **92**: 946–955.

Linheiro RS, Bergman CM. **2012**. Whole Genome Resequencing Reveals Natural Target Site Preferences of Transposable Elements in Drosophila melanogaster (JE Stajich, Ed.). *PLOS ONE* **7**: e30008.

Lu L, Chen J, Robb SMC, Okumoto Y, Stajich JE, Wessler SR. **2017**. Tracking the genome-wide outcomes of a transposable element burst over decades of amplification. *Proceedings of the National Academy of Sciences*: 201716459.

Luo S, Zhang H, Duan Y, Yao X, Clark AG, Lu J. **2020**. The evolutionary arms race between transposable elements and piRNAs in Drosophila melanogaster. *BMC Evolutionary Biology* **20**: 14.

Lynch M. **2007**. *The Origins of Genome Architecture*. Sunderland MA: Sinauer Associates.

McDonald BA, Mundt CC, Chen R. **1996**. The role of selection on the genetic structure of pathogen populations : Evidence from field experiments with Mycosphaerella graminicola on wheat. *Euphytica* **92**: 73–80.

McKenna A, Hanna M, Banks E, Sivachenko A, Cibulskis K, Kernytsky A, Garimella K, Altshuler D, Gabriel S, Daly M, *et al.* 2010. The Genome Analysis Toolkit: A MapReduce framework for analyzing next-generation DNA sequencing data. *Genome Research* **20**: 1297–1303.

Meile L, Croll D, Brunner PC, Plissonneau C, Hartmann FE, McDonald BA, Sánchez-Vallet A. **2018**. A fungal avirulence factor encoded in a highly plastic genomic region triggers partial resistance to septoria tritici blotch. *New Phytologist* **219**: 1048–1061.

Miga KH, Koren S, Rhie A, Vollger MR, Gershman A, Bzikadze A, Brooks S, Howe E, Porubsky D, Logsdon GA, *et al.* 2020. Telomere-to-telomere assembly of a complete human X chromosome. *Nature* **585**: 79–84.

Mikheenko A, Prjibelski A, Saveliev V, Antipov D, Gurevich A. **2018**. Versatile genome assembly evaluation with QUAST-LG. *Bioinformatics* **34**: i142–i150.

Nagarajan N, Pop M. **2013**. Sequence assembly demystified. *Nature Reviews Genetics* **14**: 157–167.

Nelson MG, Linheiro RS, Bergman CM. **2017**. McClintock: An Integrated Pipeline for Detecting Transposable Element Insertions in Whole-Genome Shotgun Sequencing Data. *G3: Genes|Genomes|Genetics* **7**: 2763–2778.

Odorizzi G, Babst M, Emr SD. **2000**. Phosphoinositide signaling and the regulation of membrane trafficking in yeast. *Trends in Biochemical Sciences* **25**: 229–235.

Oliver KR, McComb JA, Greene WK. **2013**. Transposable elements: Powerful contributors to angiosperm evolution and diversity. *Genome Biology and Evolution* **5**: 1886–1901.

Omrane S, Audéon C, Ignace A, Duplaix C, Aouini L, Kema G, Walker A-S, Fillinger S. **2017**. Plasticity of the MFS1 promoter leads to multi drug resistance in the wheat pathogen Zymoseptoria tritici. *mSphere*: 1–42.

Omrane S, Sghyer H, Audeon C, Lanen C, Duplaix C, Walker AS, Fillinger S. **2015**. Fungicide efflux and the MgMFS1 transporter contribute to the multidrug resistance phenotype in Zymoseptoria tritici field isolates. *Environmental Microbiology* **17**: 2805–2823.

Peter M, Kohler A, Ohm RA, Kuo A, Krützmann J, Morin E, Arend M, Barry KW, Binder M, Choi C, *et al.* 2016. Ectomycorrhizal ecology is imprinted in the genome of the dominant symbiotic fungus Cenococcum geophilum. *Nature Communications* **7**: 1–15.

Petrov DA, Aminetzach YT, Davis JC, Bensasson D, Hirsh AE. **2003**. Size matters: Non-LTR retrotransposable elements and ectopic recombination in Drosophila. *Molecular Biology and Evolution* **20**: 880–892.

Plissonneau C, Stürchler A, Croll D. **2016**. The Evolution of Orphan Regions in Genomes of a Fungal Pathogen of Wheat. *mBio* **7**: 1–13.

Quinlan AR, Hall IM. **2010**. BEDTools: A flexible suite of utilities for comparing genomic features. *Bioinformatics* **26**: 841–842.

R Core Team. **2017**. R: A language and environment for statistical computing. R Foundation for Statistical Computing, Vienna, Austria.

Raffaele S, Kamoun S. **2012**. Genome evolution in filamentous plant pathogens: why bigger can be better. *Nature Reviews Microbiology* **10**: 417–430.

Rice P, Longden L, Bleasby A. **2000**. EMBOSS: The European Molecular Biology Open Software Suite. *Trends in Genetics* **16**: 276–277.

Ritz C, Streibig JC. **2005**. Bioassay analysis using R. *Journal of Statistical Software* **12**: 1–22.

Rogers J, Gibbs RA. **2014**. Content and Dynamics. *Nature Reviews Genetics* **15**: 347–359.

Rouxel T, Grandaubert J, Hane JK, Hoede C, van de Wouw AP, Couloux A, Dominguez V, Anthouard V, Bally P, Bourras S, *et al.* 2011. Effector diversification within compartments of the Leptosphaeria maculans genome affected by Repeat-Induced Point mutations. *Nature communications* **2**: 202.

Sabeti PC, Varilly P, Fry B, Lohmueller J, Hostetter E, Cotsapas C, Xie X, Byrne EH, McCarroll SA, Gaudet R, *et al.* 2007. Genome-wide detection and characterization of positive selection in human populations. *Nature* **449**: 913–918.

SanMiguel P, Gaut BS, Tikhonov A, Nakajima Y, Bennetzen JL. **1998**. The paleontology of intergene retrotransposons of maize. *Nature Genetics* **20**: 43–45.

Shen RM, Batzer MA, Deininger PL. **1991**. Evolution of the master Alu gene(s). *Journal of Molecular Evolution* **33**: 311–320.

Simão FA, Waterhouse RM, Ioannidis P, Kriventseva E V., Zdobnov EM. **2015**. BUSCO: Assessing genome assembly and annotation completeness with single-copy orthologs. *Bioinformatics* **31**: 3210–3212.

Slotkin RK, Martienssen R. **2007**. Transposable elements and the epigenetic regulation of the genome. *Nature Reviews Genetics* **8**: 272–285.

Stöver BC, Müller KF. **2010**. TreeGraph 2: Combining and visualizing evidence from different phylogenetic analyses. *BMC Bioinformatics* **11**: 1–9.

Stritt C, Gordon SP, Wicker T, Vogel JP, Roulin AC. **2017**. Recent activity in expanding populations and purifying selection have shaped transposable element landscapes across natural accessions of the Mediterranean grass Brachypodium distachyon. *Genome Biology and Evolution* **10**: 1–38.

Stuart T, Eichten SR, Cahn J, Karpievitch Y V, Borevitz JO, Lister R. **2016**. Population scale

815 mapping of transposable element diversity reveals links to gene regulation and epigenomic
816 variation. *eLife* **5**: 1–27.

817 **Stukenbrock EH, Banke S, Javan-Nikkhah M, McDonald BA**. **2007**. Origin and domestication of
818 the fungal wheat pathogen Mycosphaerella graminicola via sympatric speciation. *Molecular*
819 *Biology and Evolution* **24**: 398–411.

820 **Torriani SFF, Melichar JPE, Mills C, Pain N, Sierotzki H, Courbot M**. **2015**. Zymoseptoria tritici:
821 A major threat to wheat production, integrated approaches to control. *Fungal Genetics and Biology*
822 **79**: 8–12.

823 **Walser J-C, Chen B, Feder ME**. **2006**. Heat-Shock Promoters: Targets for Evolution by P
824 Transposable Elements in Drosophila. *PLOS Genetics* **2**: e165.

825 **Waterhouse AM, Procter JB, Martin DMA, Clamp M, Barton GJ**. **2009**. Jalview Version 2-A
826 multiple sequence alignment editor and analysis workbench. *Bioinformatics* **25**: 1189–1191.

827 **Wickham H**. **2016**. *ggplot2: Elegant Graphics for Data Analysis*. New York: Springer-Verlag.

828 **Wickham H, Chang W**. **2016**. devtools: Tools to Make Developing R Packages Easier.

829 **Wong WY, Simakov O, Bridge DM, Cartwright P, Bellantuono AJ, Kuhn A, Holstein TW,**
830 **David CN, Steele RE, Martínez DE**. **2019**. Expansion of a single transposable element family is
831 associated with genome-size increase and radiation in the genus Hydra. *Proceedings of the*
832 *National Academy of Sciences* **116**: 22915–22917.

833 **Zhan J, Kema GHJ, Waalwijk C, McDonald BA**. **2002**. Distribution of mating type alleles in the
834 wheat pathogen Mycosphaerella graminicola over spatial scales from lesions to continents. *Fungal*
835 *Genetics and Biology* **36**: 128–136.

836 **Zhan J, Linde CC, Jurgens T, Merz U, Steinebrunner F, McDonald BA**. **2005**. Variation for
837 neutral markers is correlated with variation for quantitative traits in the plant pathogenic fungus
838 Mycosphaerella graminicola. *Mol Ecol* **14**: 2683–2693.

839 **Zhan J, Pettway RE, McDonald BA**. **2003**. The global genetic structure of the wheat pathogen
840 Mycosphaerella graminicola is characterized by high nuclear diversity, low mitochondrial
841 diversity, regular recombination, and gene flow. *Fungal Genetics and Biology* **38**: 286–297.

842 **Zheng X, Gogarten SM, Lawrence M, Stilp A, Conomos MP, Weir BS, Laurie C, Levine D**. **2017**.
843 SeqArray-a storage-efficient high-performance data format for WGS variant calls. *Bioinformatics*
844 **33**: 2251–2257.

845 **Zheng X, Levine D, Shen J, Gogarten SM, Laurie C, Weir BS**. **2012**. A high-performance
846 computing toolset for relatedness and principal component analysis of SNP data. *Bioinformatics*
847 **28**: 3326–3328.

848

849

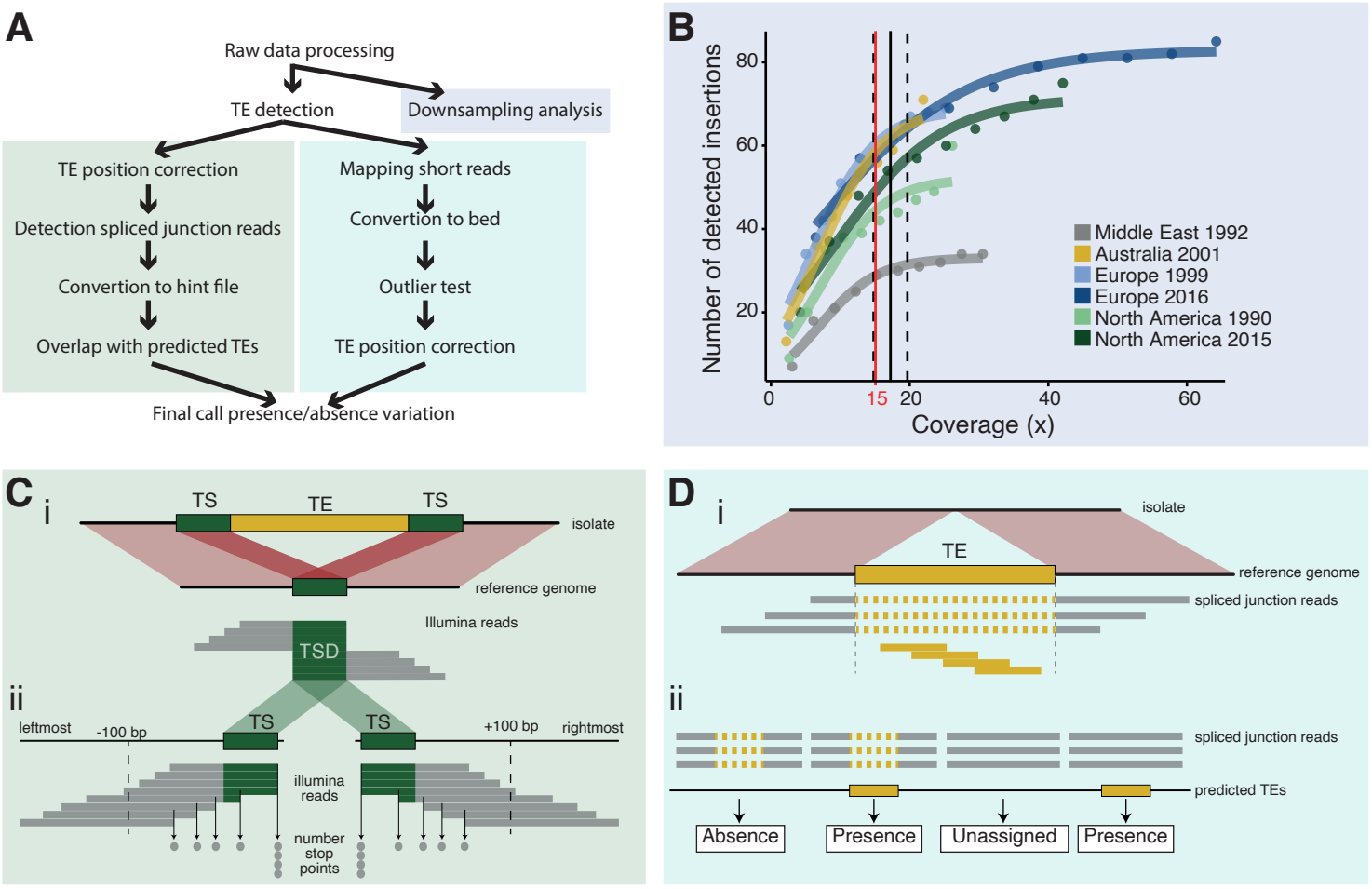
A
Raw data processing
TE detection
Downsampling analysis
TE position correction
Detection spliced junction reads
Convertion to hint file
Overlap with predicted TEs
Mapping short reads
Convertion to bed
Outlier test
TE position correction
Final call presence/absence variation
B
Number of detected insertions
Coverage (x)
Middle East 1992
Australia 2001
Europe 1999
Europe 2016
North America 1990
North America 2015
C
i
TS
TE
TS
isolate
reference genome
Illumina reads
TSD
ii
leftmost
-100 bp
TS
TS
+100 bp
rightmost
illumina reads
number stop points
D
i
isolate
TE
reference genome
spliced junction reads
ii
spliced junction reads
predicted TEs
Absence
Presence
Unassigned
Presence

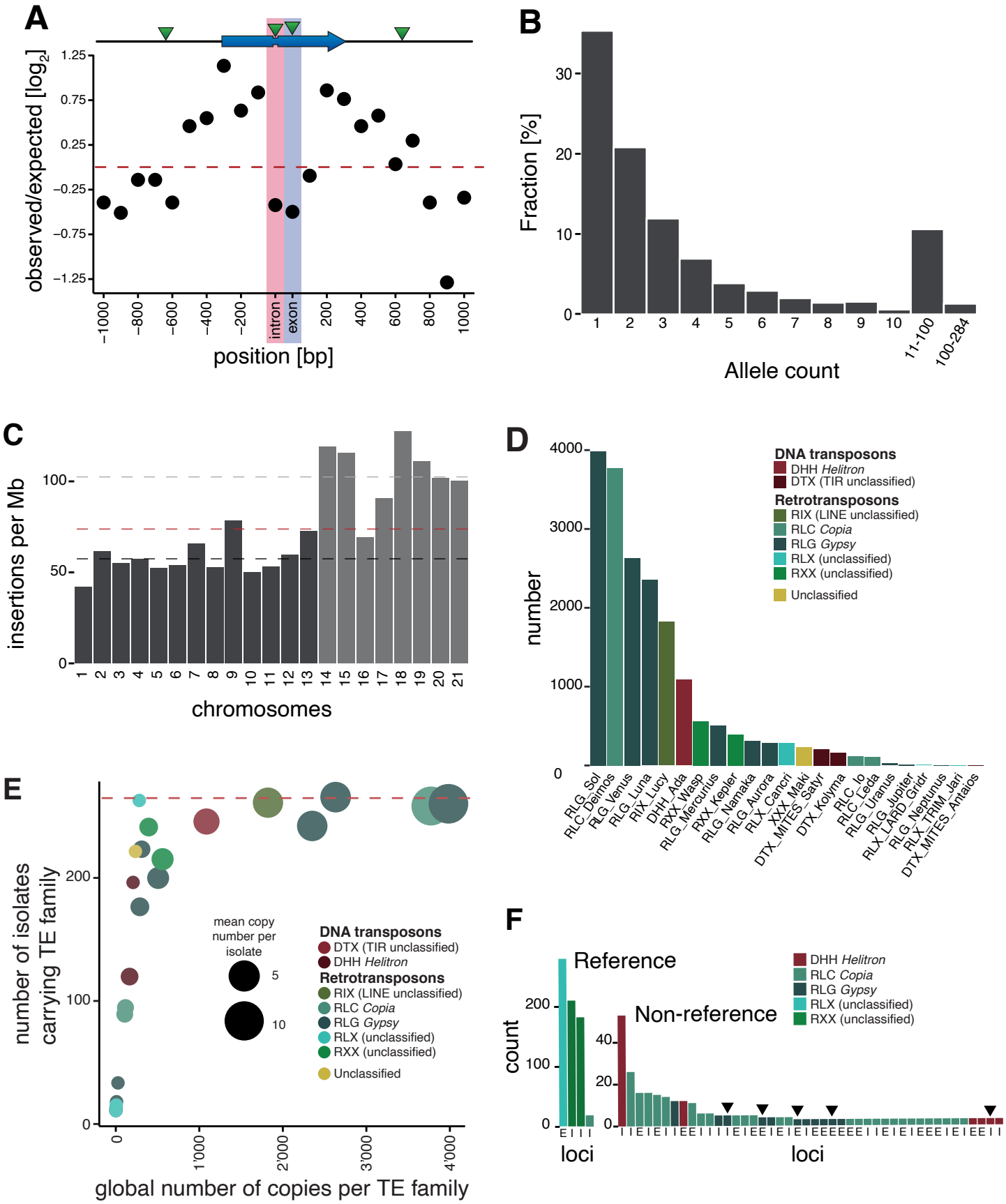
A
observed/expected [log2]
1.25
0.75
0.25
−0.25
−0.75
−1.25
−1000
−800
−600
−400
−200
intron
exon
200
400
600
800
1000
position [bp]
B
Fraction [%]
30
20
10
0
1
2
3
4
5
6
7
8
9
10
11-100
100-284
Allele count
C
insertions per Mb
100
50
0
1
2
3
4
5
6
7
8
9
10
11
12
13
14
15
16
17
18
19
20
21
chromosomes
D
number
4000
3000
2000
1000
0
DNA transposons
DHH Helitron
DTX (TIR unclassified)
Retrotransposons
RIX (LINE unclassified)
RLC Copia
RLG Gypsy
RLX (unclassified)
RXX (unclassified)
Unclassified
RLG_Sol
RLC_Deimos
RLG_Venus
RLG_Luna
RIX_Lucy
DHH_Ada
RXX_Wasp
RLG_Mercurius
RXX_Kepler
RLG_Namaka
RLG_Aurora
RLX_Cancri
XXX_Maki
DTX_MITES_Satyr
DTX_Kolyma
RLC_Io
RLC_Leda
RLG_Uranus
RLG_Jupiter
RLX_LARD_Gridr
RLG_Neptunus
RLX_TRIM_Jari
DTX_MITES_Antaios
E
number of isolates carrying TE family
200
100
0
mean copy number per isolate
5
10
DNA transposons
DTX (TIR unclassified)
DHH Helitron
Retrotransposons
RIX (LINE unclassified)
RLC Copia
RLG Gypsy
RLX (unclassified)
RXX (unclassified)
Unclassified
0
1'000
2'000
3'000
4'000
global number of copies per TE family
F
Reference
Non-reference
count
200
100
0
40
20
0
DHH Helitron
RLC Copia
RLG Gypsy
RLX (unclassified)
RXX (unclassified)
E I I I
I I E I E I I E E I I I I E I E E I E I E E E E E I I E I E I E E I E I E E I I
loci
loci

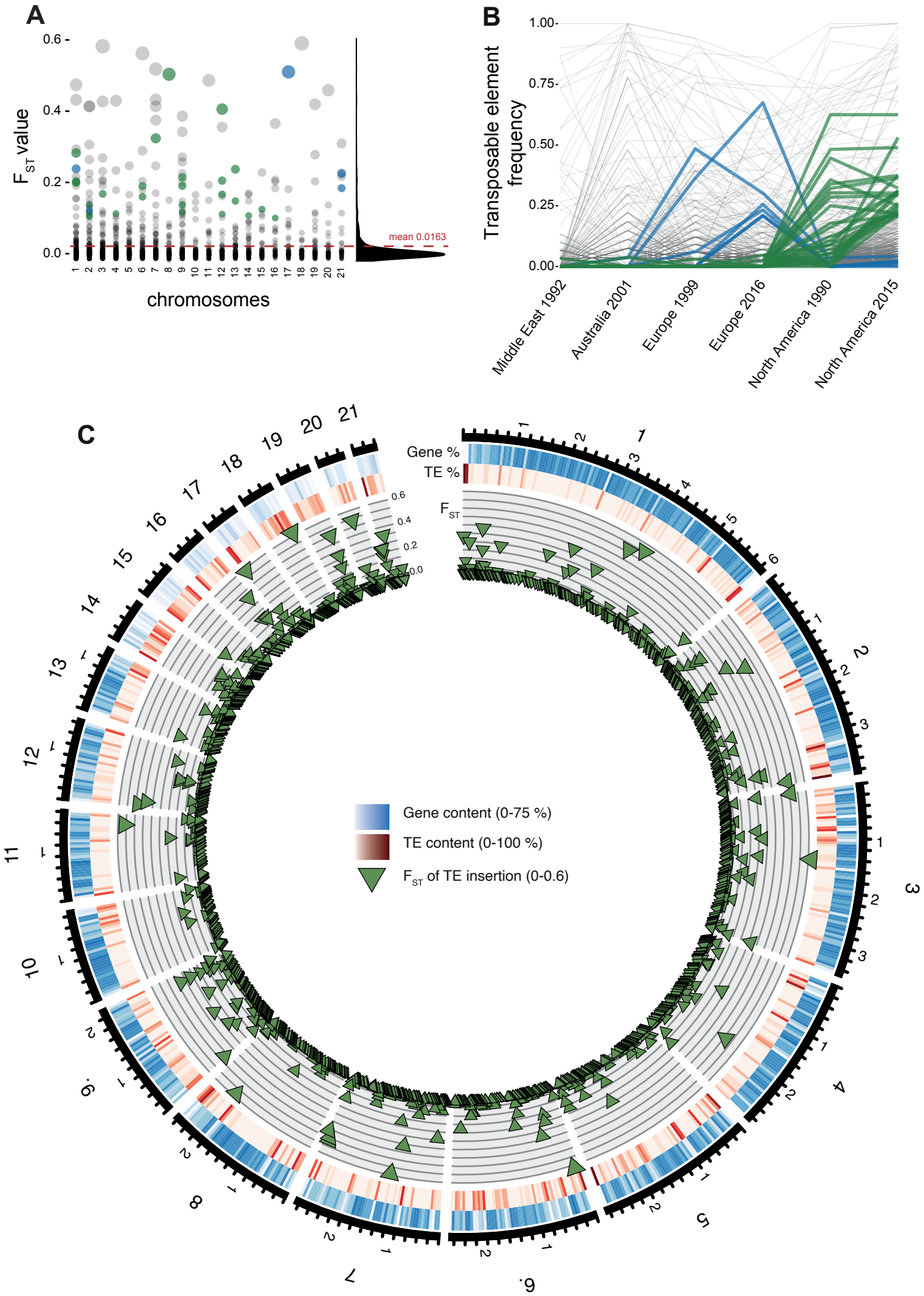
A
0.6
0.4
0.2
0.0
F_{ST} value
mean 0.0163
chromosomes
B
1.00
0.75
0.50
0.25
0.00
Transposable element frequency
Middle East 1992
Australia 2001
Europe 1999
Europe 2016
North America 1990
North America 2015
C
Gene %
TE %
F_{ST}
Gene content (0-75 %)
TE content (0-100 %)
F_{ST} of TE insertion (0-0.6)

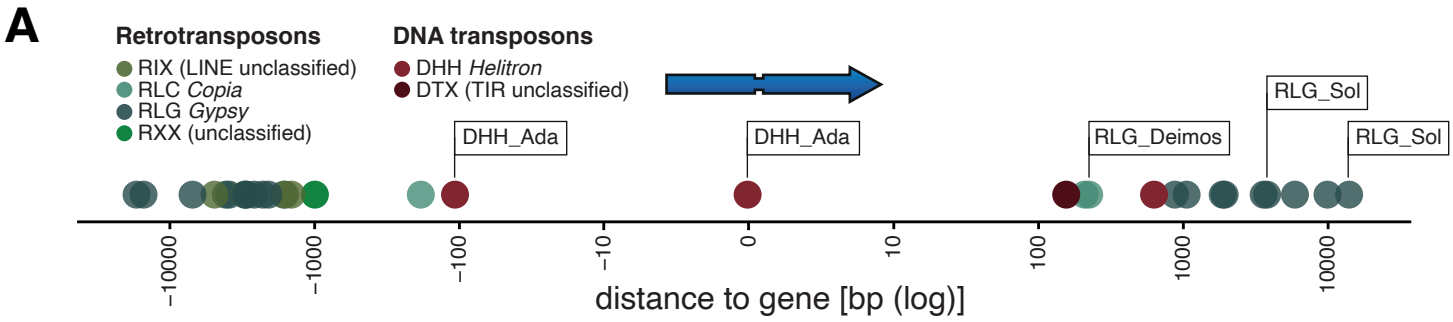
A
Retrotransposons
RIX (LINE unclassified)
RLC Copia
RLG Gypsy
RXX (unclassified)
DNA transposons
DHH Helitron
DTX (TIR unclassified)
DHH_Ada
DHH_Ada
RLG_Deimos
RLG_Sol
RLG_Sol
−10000
−1000
−100
−10
0
10
100
1000
10000
distance to gene [bp (log)]

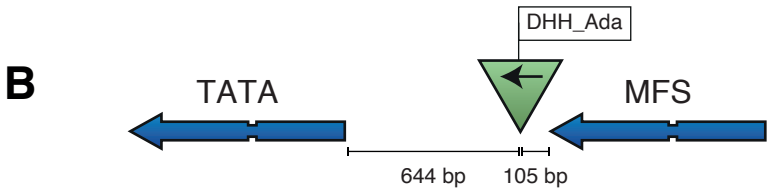
B
DHH_Ada
TATA
MFS
644 bp
105 bp

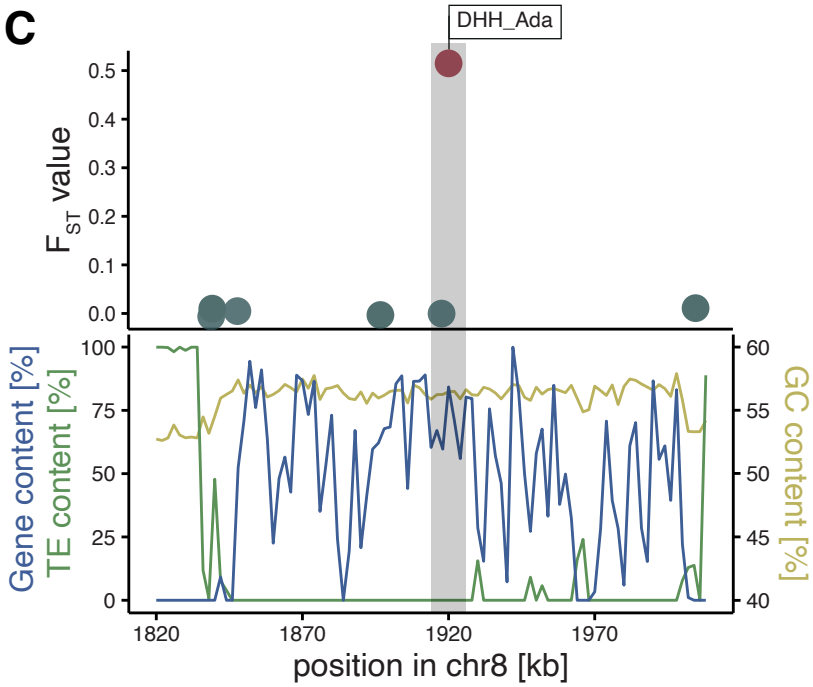
C
DHH_Ada
F_ST value
0.5
0.4
0.3
0.2
0.1
0.0
Gene content [%]
TE content [%]
GC content [%]
100
75
50
25
0
60
55
50
45
40
1820
1870
1920
1970
position in chr8 [kb]

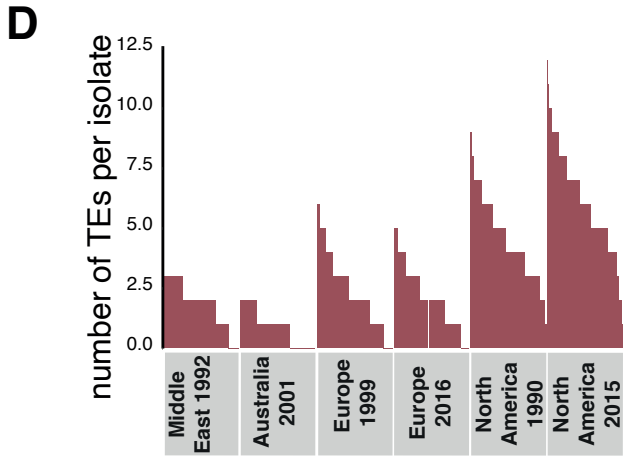
D
number of TEs per isolate
12.5
10.0
7.5
5.0
2.5
0.0
Middle East 1992
Australia 2001
Europe 1999
Europe 2016
North America 1990
North America 2015

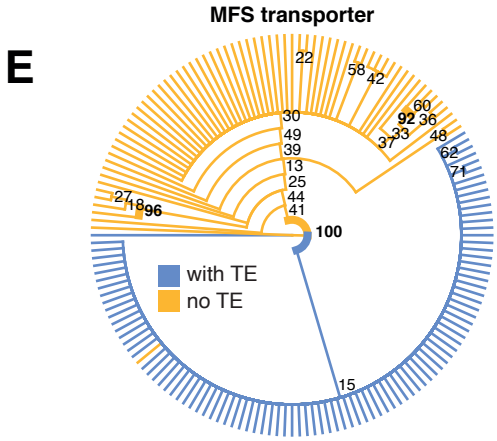
E
MFS transporter
with TE
no TE

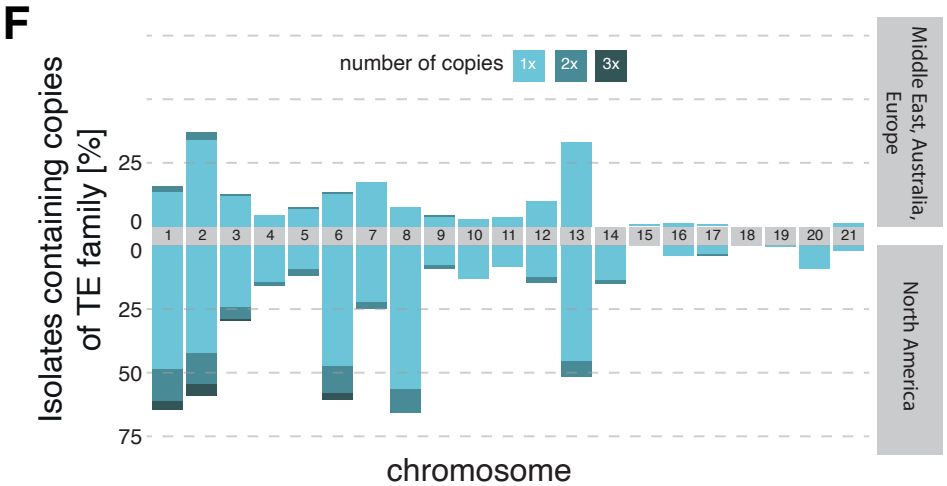
F
number of copies
1x
2x
3x
Isolates containing copies of TE family [%]
25
0
0
25
50
75
1
2
3
4
5
6
7
8
9
10
11
12
13
14
15
16
17
18
19
20
21
Middle East, Australia, Europe
North America
chromosome

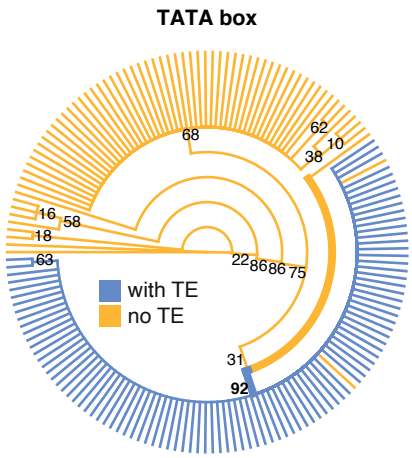
TATA box
with TE
no TE

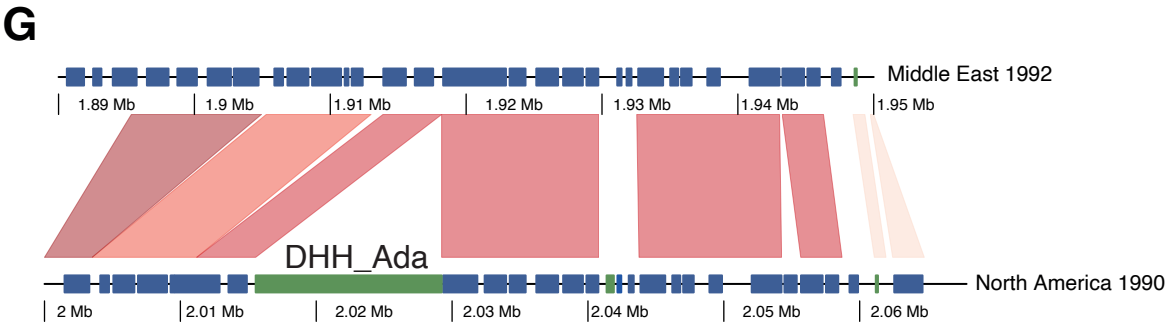
G
Middle East 1992
1.89 Mb
1.9 Mb
1.91 Mb
1.92 Mb
1.93 Mb
1.94 Mb
1.95 Mb
DHH_Ada
North America 1990
2 Mb
2.01 Mb
2.02 Mb
2.03 Mb
2.04 Mb
2.05 Mb
2.06 Mb

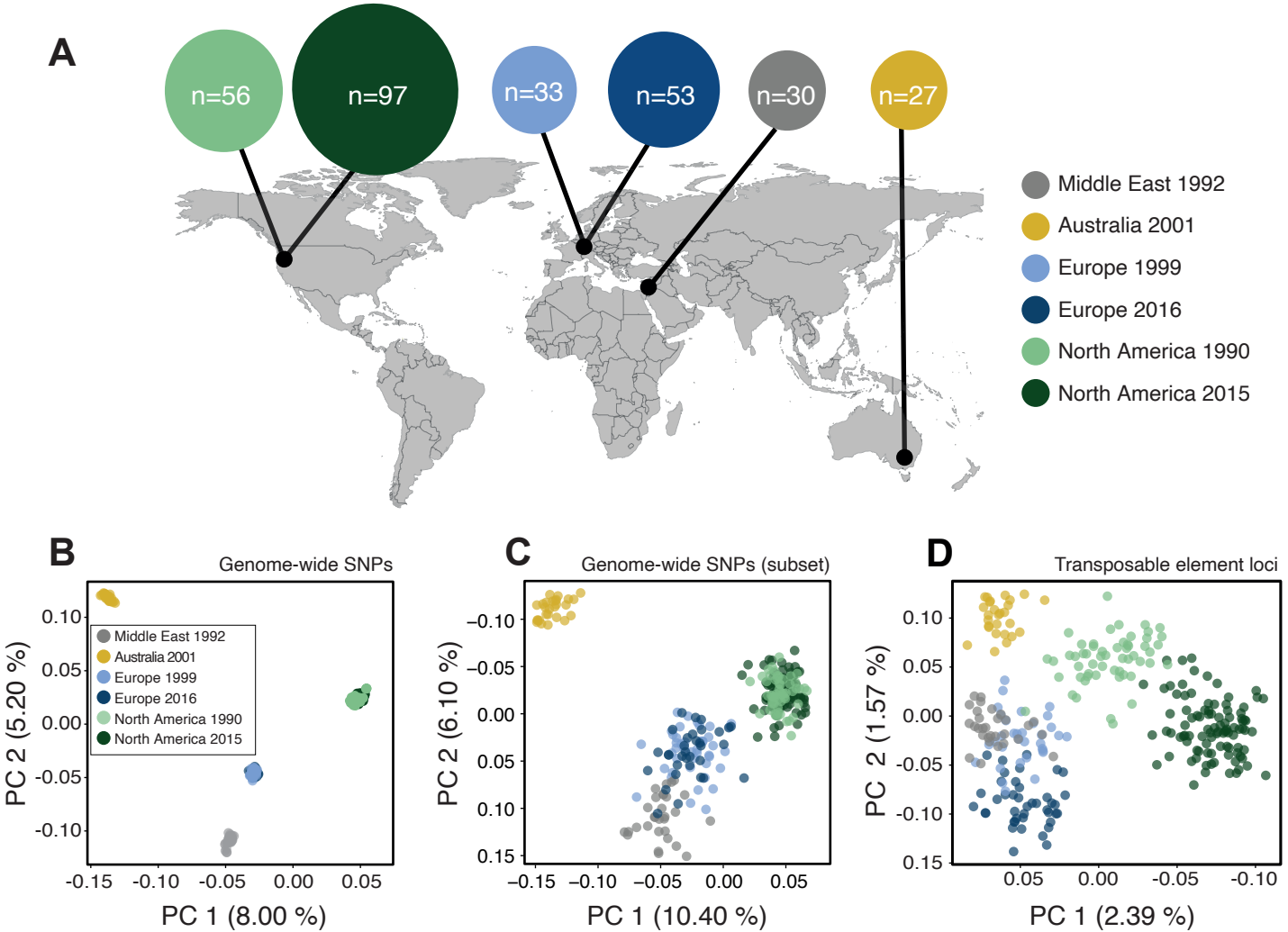
A
n=56
n=97
n=33
n=53
n=30
n=27
Middle East 1992
Australia 2001
Europe 1999
Europe 2016
North America 1990
North America 2015
B
Genome-wide SNPs
Middle East 1992
Australia 2001
Europe 1999
Europe 2016
North America 1990
North America 2015
PC 2 (5.20 %)
PC 1 (8.00 %)
C
Genome-wide SNPs (subset)
PC 2 (6.10 %)
PC 1 (10.40 %)
D
Transposable element loci
PC 2 (1.57 %)
PC 1 (2.39 %)

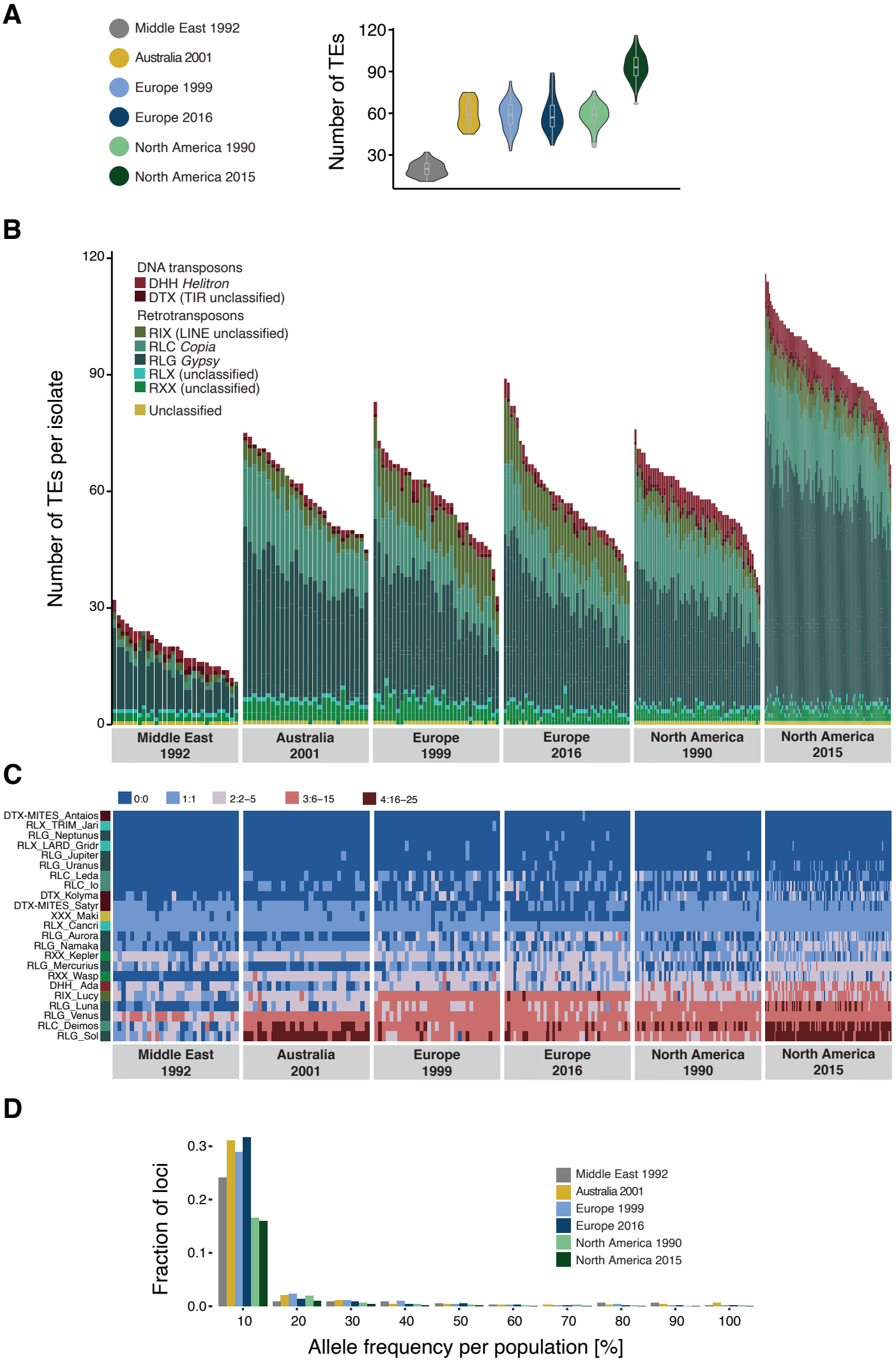
A
Middle East 1992
Australia 2001
Europe 1999
Europe 2016
North America 1990
North America 2015
Number of TEs
120
90
60
30
B
DNA transposons
DHH Helitron
DTX (TIR unclassified)
Retrotransposons
RIX (LINE unclassified)
RLC Copia
RLG Gypsy
RLX (unclassified)
RXX (unclassified)
Unclassified
Number of TEs per isolate
120
90
60
30
0
Middle East 1992
Australia 2001
Europe 1999
Europe 2016
North America 1990
North America 2015
C
0:0
1:1
2:2–5
3:6–15
4:16–25
DTX-MITES_Antaios
RLX_TRIM_Jari
RLG_Neptunus
RLX_LARD_Gridr
RLG_Jupiter
RLG_Uranus
RLC_Leda
RLC_Io
DTX_Kolyma
DTX-MITES_Satyr
XXX_Maki
RLX_Cancri
RLG_Aurora
RLG_Namaka
RXX_Kepler
RLG_Mercurius
RXX_Wasp
DHH_ Ada
RIX_Lucy
RLG_Luna
RLG_Venus
RLC_Deimos
RLG_Sol
Middle East 1992
Australia 2001
Europe 1999
Europe 2016
North America 1990
North America 2015
D
Fraction of loci
0.3
0.2
0.1
0.0
Middle East 1992
Australia 2001
Europe 1999
Europe 2016
North America 1990
North America 2015
10
20
30
40
50
60
70
80
90
100
Allele frequency per population [%]

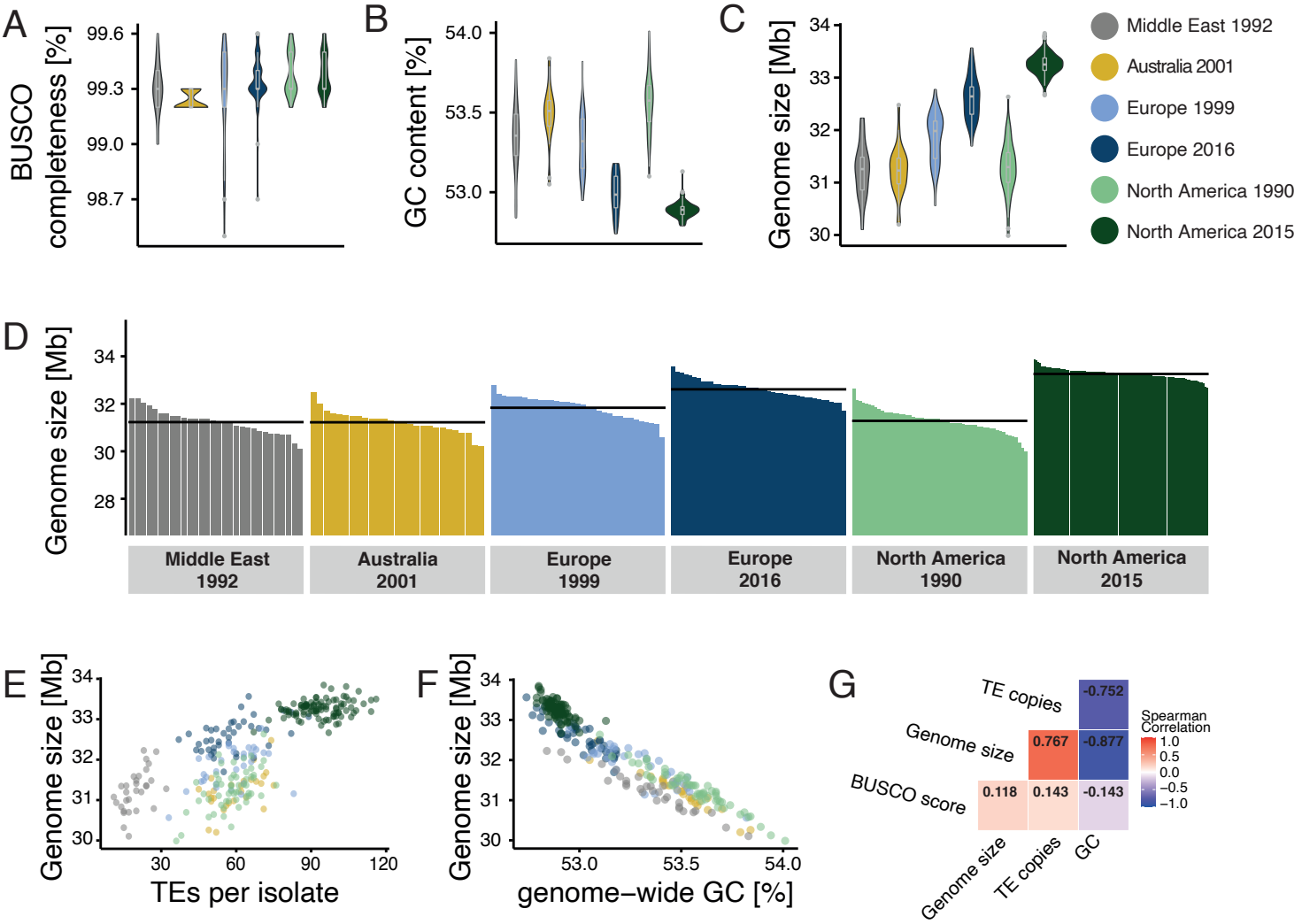
A
BUSCO completeness [%]
99.6
99.3
99.0
98.7
B
GC content [%]
54.0
53.5
53.0
C
Genome size [Mb]
34
33
32
31
30
Middle East 1992
Australia 2001
Europe 1999
Europe 2016
North America 1990
North America 2015
D
Genome size [Mb]
34
32
30
28
Middle East 1992
Australia 2001
Europe 1999
Europe 2016
North America 1990
North America 2015
E
Genome size [Mb]
TEs per isolate
30
60
90
120
F
Genome size [Mb]
genome−wide GC [%]
53.0
53.5
54.0
G
TE copies
Genome size
BUSCO score
-0.752
0.767
-0.877
0.118
0.143
-0.143
Genome size
TE copies
GC
Spearman Correlation
1.0
0.5
0.0
−0.5
−1.0